IEEE Open Journal of the Communications Society

Received 27 September 2023; accepted 14 October 2023. Date of publication 24 October 2023; date of current version 27 November 2023.

Digital Object Identifier 10.1109/OJCOMS.2023.3326340

Proactive Eavesdropping Performance for Integrated Satellite–Terrestrial Relay Networks

ZHEPING WU[1], KEFENG GUO[2], XINGWANG LI[3,4] (Senior Member, IEEE), YU-DONG ZHANG[5] (Senior Member, IEEE), MINGFU ZHU[6] (Member, IEEE), HOUBING SONG[7] (Fellow, IEEE), AND MIN WU[2]

[1]Naval Submarine Academy, Qingdao 266199, China
[2]School of Space Information, Space Engineering University, Beijing 101407, China
[3]School of Physics and Electronics Information Engineering, Henan Polytechnic University, Jiaozuo 454000, China
[4]Jiaozuo Key Laboratory of Crow-Sensing Network, Jiaozuo 454003, China
[5]School of Computing and Mathematics, University of Leicester, LE1 7RH Leicester, U.K.
[6]School of Computer Science and Technology, Henan Polytechnic University, Jiaozuo 454000, China
[7]Department of Information Systems, University of Maryland at Baltimore County, Baltimore, MD 21250, USA

CORRESPONDING AUTHOR: K. GUO (e-mail: guokefeng.cool@163.com)

This work was supported by the Research Project of Space Engineering University under Grant 2020XXAQ01.

ABSTRACT This work investigates the proactive eavesdropping based legitimate surveillance for integrated satellite-terrestrial relay networks with multiple proactive monitors. To study the eavesdropping non-outage probability, we propose three different presentative proactive eavesdropping cases/modes, where the legitimate monitors could change its roles between eavesdropping and jamming, namely, Case I: Eavesdropping then Jamming, Case II: Jamming then Eavesdropping, Case III: Always Eavesdropping. Particularly, we get the accurate expressions of the eavesdropping non-outage probability for the proposed three proactive eavesdropping modes in the presence of multiple monitors. To derive further insights, we provide the asymptotic analysis of the three eavesdropping non-outage probabilities. Besides, the colluding proactive eavesdropping scenario is considered, in which all the monitors cooperate to overhear or jam the legitimate users. Finally, numerical results are obtained to verify the rightness of the analytical analysis.

INDEX TERMS Integrated satellite-terrestrial relay networks (ISTRNs), proactive multiple monitors, three proactive eavesdropping modes, eavesdropping non-outage probability.

I. INTRODUCTION

THE INCREASING requirements for large data transmission and wide coverage in the next wireless communication systems are the major challenges, especially for the beyond the 5-th generation (B5G) networks even the 6-th generation (6G) networks. Focusing on this front, the satellite-terrestrial networks (STNs) have been paid significant attentions, which can overcome the shortages of terrestrial networks, for example, it is restricted by terrain, and having low coverage [1], [2], [3], [4]. By considering some obstacles and heavy showings in STNs, the integrated satellite-terrestrial relay networks (ISTRNs) have been viewed as the more promising framework to provide an enhanced coverage, data transmission rate, and the other 6G networks requirements, which is considered as the major part of the Internet of Things (IoT) networks [5], [6], [7], [8]. The ISTRN's framework has been regarded as an important factor of the satellite communications (SatComs) that uses the terrestrial nodes to enhance the satellite transmission, which is often utilized into the mobile/fixed satellite systems, such as SiriusXM [9]. It has become a realistic case which has been included in Digital Video Broadcasting (DVB) networks [10]. Besides, ISTRNs are also contained in "Space-Ground Integrated Information Network Engineering" of China [11].

A. RELATED STUDIES

Till now, outage probability (OP), throughput and the other performance metrics of ISTRNs have been investigated by existing literatures. The authors in [12] researched the OP for an ISTRN with a relay. The work in [13] researched the OP of a cognitive ISTRN with multiple interferences. In [14], the authors utilized a terrestrial relay selection algorithm in an uplink ISTRN with several terrestrial relays and hardware impairments. In [15], the authors utilized a joint optimization scheme for the non-orthogonal multiple access (NOMA)-assisted ISTRNs. The authors in [16] researched the performance of a multiuser ISTRN, particularly, the accurate expression for OP was further investigated. Through [17], the authors researched energy efficient algorithm for a satellite-aerial-terrestrial network (SATN), where the relay, i.e., the multi-antenna unmanned aerial vehicle (UAV) is utilized to assist the satellite to transmit the information. The authors in [18] researched the effects of channel estimation errors (CEEs) and hardware impairments (HIs) on the NOMA-based cognitive ISTRNs, especially, the secrecy outage probability (SOP) was further studied. In [19], the authors used the transmit antenna selection scheme on the NOMA-assisted ISTRNs with imperfect CEEs and non-ideal successive interference cancellation (SIC). In [20], the authors researched the impact of NOMA on the secrecy performance for the ISTRNs.

It is essential to monitor and legitimately eavesdrop on some suspicious wireless communication, like illegal eavesdropping, mass text, and tampering with communication content, to deal with the case that high-risk events [20], [21]. For the wireless surveillance, it could be divided into two scenarios. First scenario is passive eavesdropping, which means the legitimate monitor only overhears the suspicious transmission link. In this scenario, the perfect channel state information (CSI) for each related channel is considered. This scenario works only at the case that the performance of eavesdropping link is preferable to that of the suspicious link. Some related works have investigated the secrecy problem in ISTRNs on the passive eavesdropping scenario [22], [23], [24], [25], [26], [27]. The authors in [22] utilized a threshold-based legitimate user scheduling algorithm and analyzed the secrecy performance for ISTRNs. The authors in [23] researched the secure transmission for the cognitive ISTRNs. In [24], the secrecy performance for the NOMA-assisted ISTRNs was researched, where the detailed investigations for SOP were obtained. In [25], the authors researched the secrecy performance of a downlink ISTRN, where the SOP was investigated with respect to the detailed analysis. In [26], the authors proposed a max user scheduling algorithm for the SatCom, moreover, the SOP was further researched. The authors in [28] researched the SOP for an ISTRN along with several two-way terrestrial nodes. Except the performance, the secrecy beamforming for the ISTRNs is also the popular topic [15], [29], [30]. In these papers, the secrecy performance is optimized through different optimization methods.

B. MOTIVATIONS

However, in practical systems, this situation can not be satisfied for the reason that the monitor has a long distance with the suspicious transmitter to avoid being found. To solve this problem, the authors in [31] proposed another scenario with its name as proactive eavesdropping scenario. In this scenario, the monitor has the ability that receives the suspicious signals and sends the jamming information at the same time with a full-duplex mode. With the help of the jamming information, the transmission rate of the suspicious signals can be decreased. In addition, it also can enhance the eavesdropping even though the channel property for the eavesdropping link is worse than that of suspicious links without jamming. The authors considered a three-node surveillance rate maximization problem in [32]. On this foundation, the authors in [33] extended the work of [31] by assuming the suspicious transceiver and the monitor equipped with several antennas. The authors in [34] investigated the proactive eavesdropping problem by utilizing the amplify-and-forward relay scheme. In [35], the authors researched a novel wireless surveillance scenario with a reconfigurable intelligent surface (RIS). In [36], the authors proposed a novel objective of eavesdropping energy utilization rate to valuate the eavesdropping quality. The authors in [37] researched the impact of RIS on the proactive eavesdropping case relied on the deep reinforcement learning method. Reference [38] optimized the power and location for the proactive eavesdropping networks with a full-duplex terrestrial relay. In [31], the authors studied the proactive eavesdropping via jamming through the Rayleigh fading channel, especially, the rate maximization was further researched. In [39], the authors utilized the mode selection algorithm for the proactive eavesdropping with jamming to get the best eavesdropping performance. In [40], the authors researched the energy utilization rate for the proactive eavesdropping. In [41], the authors investigated the fairness problems for the UAV-based networks. In [42], the authors still studied the proactive eavesdropping problems for the UAV-based communications. In [43], the proactive problem is analyzed in the full-duplex communication systems along with the multiple antenna node. In [39], the authors researched the mode selection problem for the proactive eavesdropping scheme. In [44], the authors investigated the proactive eavesdropping performance for the 5G uplink systems. especially the multiple antennas were considered. In [45], the authors analyzed the proactive eavesdropping performance for the simultaneously transmitting and reflecting-RIS based networks with statistical CSI.

As mentioned before, ISTRNs and proactive eavesdropping are considered as the major parts for the next wireless transmission networks, thus it is very important for us to investigate the performance of proactive eavesdropping in the ISTRNs. Until now, only the authors in [46] investigated the proactive eavesdropping performance for the ISTRNs with eavesdropping then jamming scenario, which indicates the importance and necessity of our research.

C. OUR CONTRIBUTIONS

However, as the authors know that the investigation of proactive eavesdropping on the ISTRNs has not been published, which motivates our work. Specifically, the major contributions are given in the following:

- Firstly, this paper illustrates a general proactive eavesdropping model for the ISTRNs, where a suspicious satellite, a suspicious receiver and multiple monitors are considered in this system model. This system model is new for the ISTRNs when compared with the existed works, which will be considered as the further direction for this topic.
- Secondly, three proactive eavesdropping cases/modes are proposed, namely, Case I: Eavesdropping then Jamming, Case II: Jamming then Eavesdropping and Case III: Always Eavesdropping. Particularly, the accurate expressions for eavesdropping non-outage probability (ENOP) for the considered three cases are obtained, which offer valuable ways to valuate the major system and channel parameters on the analyzed systems.
- Thirdly, to reduce the computational complexity and obtain further investigations of the system parameters on the system performance, the approximate investigations for ENOP are provided in high signal-to-noise ratio (SNR) regime.
- Some representative simulation results are obtained to prove the analytical results. With these results, the effects of the system parameters are shown with the clear view.

The left parts are organized as what follows. In Section II, the illustration of the considered system model is introduced. In Section III, the detailed process for the power control and ENOP is obtained along with the three proposed proactive eavesdropping cases/modes. In Section IV, Monte Carlo (MC) simulations are given to verify the theoretical results. In Section V, the conclusion is obtained to end the whole paper.

Notations: $E[\cdot]$ is the expectation operator, $\exp(\cdot)$ denotes the exponential function. The abbreviations and acronyms are provided in TABLE 1, shown at the top of next page.

TABLE 1. Acronyms and abbreviations.

Acronym	Definition
B5G	beyond the 5-th generation
STN	satellite-terrestrial networks
ISTRNs	integrated satellite-terrestrial relay networks
IoT	Internet of Things
DVB	Digital Video Broadcasting
OP	outage probability
NOMA	non-orthogonal multiple access
SATN	satellite-aerial-terrestrial network
UAV	unmanned aerial vehicle
CEEs	channel estimation errors
HIs	hardware impairments
SOP	secrecy outage probability
SIC	successive interference cancellation
CSI	channel state information
SatCom	satellite communication
RIS	reconfigurable intelligent surface
DF	decode-and-forward
SNR	signal-to-noise ratio
SINR	signal-to-interference plus noise ratio
AWGN	additive white Gaussian noise
ENOP	eavesdropping non-outage probability
CDF	cumulative distribution function
PDF	probability density function
GEO	geosynchronous earth orbit
TDMA	time division multiple access
FSL	free space loss
SR	shadowed-Rician
LMS	land mobile satellite
LoS	line of sight
AS	average shadowing
FHS	frequent heavy shadowing
ILS	infrequent light shadowing
MRC	maximal ratio combining
MC	Monte Carlo

II. SYSTEM DESCRIPTION

As shown in Fig. 1, we investigate the performance of proactive eavesdropping in ISTRNs, where includes a suspicious satellite (S), a suspicious terrestrial receiver (D), N monitors (E) aim to overhear or jam the information between S and D. All the legitimate monitors cooperate together to overhear or jam the signals [48], [49], [50]. A half-duplex (R) is used to forward the signal from S to D.[1] R is working with the decode-and-forward (DF) protocol. It has the assumption that all transmission nodes having the single antenna.[2] Owing to the heavy shadowing fading, the direct transmission link is not contained in this paper, which has been widely assumed in existing works [18], [19], [20].[3,4]

As a common scene, 2 time slots are required for the whole communication. During the first time slot, R receives the information of S, then transmits the decoded signal to D during the second time slot. The multiple monitors may select either jamming or eavesdropping among the two time slots, which are mainly judged by the channel quality. Three proactive eavesdropping Cases are investigated in this paper, namely Case I: Eavesdropping then Jamming,

1. Although only one terrestrial relay is employed for the considered system, the derived results can be considered as a special case of multiple terrestrial relays scenario.

2. It is mentioned that, in this paper, the terrestrial nodes are equipped with only one antenna, while the results are also suitable to the case that transmission nodes are equipped with multiple antennas and beamforming (BF) is utilized at each multiple antenna node.

3. Owing to obstacles, weather conditions like rain, fog and the other reasons, only one direct link is considered in this paper, which is a widely used assumption [18], [20].

4. In this paper, we consider that the user D was not equipped with the satellite antenna, thus it can not receive the signal from the satellite, it needs the help of the terrestrial relay.

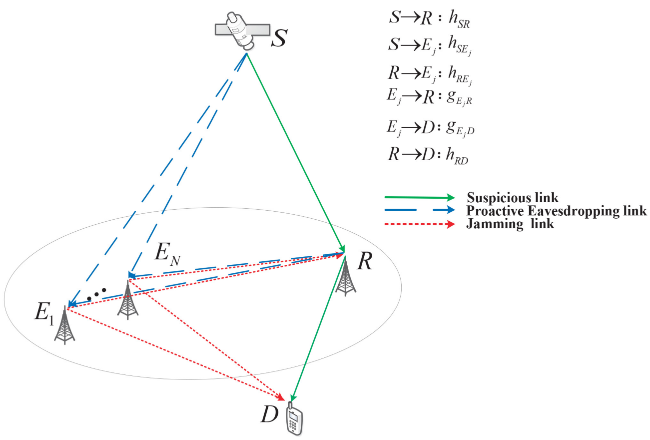

FIGURE 1. Illustration of the system model.

Case II: Jamming then Eavesdropping, and Case III: Always Eavesdropping.[5]

In Case I, during the first time slot, N monitors first eavesdrop the target signal from S, then jam the received signal at D. $s(t)$ which comes from the suspicious transmitter with $E[|s(t)|^2] = 1$ will be sent to the suspicious R, while the multiple monitors E overhear the signals. Thus, the derived signals at R and the j-th E are, respectively, obtained as

$$y_R(t) = \sqrt{P_S} h_{SR} s(t) + n_R(t), \tag{1}$$

$$y_{E_j}(t) = \sqrt{P_S} h_{SE_j} s(t) + n_{E_j}(t), \tag{2}$$

where P_S denotes the transmission power of S, h_{SR} and h_{SE_j} represent the channel fading between S and R, the channel fading between S and the j-th E, respectively, either of them suffers the shadowed-Rician (SR) fading [47]. $n_R(t)$ and $n_{E_j}(t)$ denote the additive Gaussian white noise (AWGN) at R and the j-th E, respectively, with distribution as $n_R(t) \sim \mathcal{CN}(0, \delta_R^2)$ and $n_{E_j}(t) \sim \mathcal{CN}(0, \delta_{E_j}^2)$.

By utilizing (1) and (2), the SNRs at R and the j-th E are, respectively, obtained as

$$\gamma_{SR} = P_S |h_{SR}|^2 / \delta_R^2, \tag{3}$$

$$\gamma_{SE_j} = P_S \left|h_{SE_j}\right|^2 / \delta_{E_j}^2. \tag{4}$$

As colluding scheme is utilized at the legitimate monitors, so the obtained SNR at E is given by[6]

$$\gamma_E = \gamma_{SE} = \sum_{j=1}^{N} \gamma_{SE_j}. \tag{5}$$

For the second time slot, the jamming signal $I_j(t)$ which obeys $E[|I_j(t)|^2] = 1$ with its suspicious information is transmitted by the j-th E as the destination is terrestrial receiver D. At the same time, R forwards the decoded signal to the suspicious terrestrial receiver D. By utilizing colluding scheme, the gotten signal at terrestrial receiver D is derived as

$$y_D(t) = \sqrt{P_R} h_{RD} s(t) + \sum_{j=1}^{N} \sqrt{P_{E_j}} g_{E_jD} I_j(t) + n_D(t), \tag{6}$$

where P_R and P_{E_j} represent the transmission power at R and the j-th E, respectively. h_{RD} and g_{E_jD} represent the channel coefficient between R and terrestrial receiver D, the channel coefficient between the j-th E and terrestrial receiver D, respectively, which are both modeled as Rayleigh fading. $n_D(t)$ is the AWGN at D with $n_D(t) \sim \mathcal{CN}(0, \delta_D^2)$.

By utilizing (6), the final signal-to-interference plus noise ratio (SINR) can be obtained as

$$\gamma_{D_1} = \frac{\gamma_{RD}}{\gamma_{ED} + 1}, \tag{7}$$

where $\gamma_{RD} = \frac{P_R|h_{RD}|^2}{\delta_D^2}$ and $\gamma_{ED} = \sum_{j=1}^{N} \gamma_{E_jD} = \sum_{j=1}^{N} \frac{P_{E_j}|h_{E_jD}|^2}{\delta_D^2}$.

Owing to the reason that DF protocol is utilized at R, the SINR at terrestrial receiver D is given by

$$\gamma_{F_1D} = \min\left(\gamma_{SR}, \gamma_{D_1}\right). \tag{8}$$

In Case II, in the first time slot, S forwards the signal to R, which N monitors transmit the jamming interference $I_j(t)$ to R. Thus, the signal received at R is obtained as

$$y_R(t) = \sqrt{P_S} h_{SR} s(t) + \sum_{j=1}^{N} \sqrt{P_{E_j}} g_{E_jR} I_j(t) + n_R(t), \tag{9}$$

where g_{E_jR} depicts the channel coefficient between the j-th E and R which obeys the Rayleigh fading.

Through the second time slot, R re-transmits the decoded signals to terrestrial receiver D, while at the same time, N monitors try to overhear the signals, relied on this consideration, the gotten signal at D is shown as

$$y_D(t) = \sqrt{P_R} h_{RD} s(t) + n_D(t). \tag{10}$$

By utilizing the similar way, the final SINR for Case II at R is given by

$$\gamma_{R_2} = \frac{\gamma_{SR}}{\gamma_{ER} + 1}, \tag{11}$$

where $\gamma_{ER} = \sum_{j=1}^{N} \gamma_{E_jR} = \sum_{j=1}^{N} \frac{P_{E_j}|h_{E_jR}|^2}{\delta_R^2}$.

The final SNR for the second time slot at terrestrial receiver D for Case II is obtained as

$$\gamma_{D_2} = \gamma_{RD}. \tag{12}$$

By using the DF protocol, the final SINR at terrestrial receiver D for Case II is given by

$$\gamma_{F_2D} = \min\left(\gamma_{R_2}, \gamma_{D_2}\right). \tag{13}$$

5. This system model is a general model, which not only suits for the terrestrial networks but also the vehicle networks.

6. In this paper, every node has the equal position, so all nodes can receive the interference of the monitors. This consideration has appeared in so many former papers, such as [9], [20], [51], [52]. The other reason is to simplify the analysis, thus every node is considered to have the same power, however, different eavesdropping scheme is applied into different node will be an interesting topic, which will be investigated in the near future.

By using the same method, the gotten signal for Case II at the j-th E can be obtained as

$$y_{E_j}(t) = \sqrt{P_R} h_{RE_j} s(t) + n_{E_j}(t), \tag{14}$$

where h_{RE_j} depicts the channel coefficient between R and the j-th E modeled as Rayleigh fading.

For all the monitors cooperate together [48], [49], [50], hence the SNR at E is obtained as

$$\gamma_E = \gamma_{RE} = \sum_{j=1}^{N} \gamma_{RE_j} = \sum_{j=1}^{N} \frac{P_R \left|h_{RE_j}\right|^2}{\delta_{E_j}^2}. \tag{15}$$

In Case III, the monitors only act as the eavesdropper for the whole two time slots, thus through the first time slot, the received SNR at R is obtained as

$$\gamma_{R_3} = \gamma_{SR}. \tag{16}$$

At this time, the received SNR for the first time slot at the E can be derived as

$$\gamma_{E_3} = \gamma_{SE}. \tag{17}$$

Then, for the second time slot, the derived SNR at terrestrial receiver D is represented as

$$\gamma_{D_3} = \gamma_{RD}. \tag{18}$$

The obtained SNR at the E for the second time slot is shown as

$$\gamma_{E_3} = \gamma_{RE}, \tag{19}$$

where γ_{E_3} represents the received SNR at E for Case III.

Due to the DF protocol, the final SNR for Case III at D is given by

$$\gamma_{F_3D} = \min\left(\gamma_{R_3}, \gamma_{D_3}\right). \tag{20}$$

Owing to the reason that E can receive two independent signals, thus we utilize the maximal ratio combining (MRC) algorithm to guarantee the eavesdropping performance. On this foundation, the final effective SNR at E after MRC is obtained as

$$\gamma_E = \gamma_{SE} + \gamma_{RE}. \tag{21}$$

III. POWER CONTROL AND EAVESDROPPING NON-OUTAGE PROBABILITY ANALYSIS

The power control and ENOP analysis will be given in this Section.

A. PRELIMINARY RESULTS

Before investigating the power control and performance analysis, the probability density function (PDF) and cumulative distribution function (CDF) for the transmission channels are first given.

1) SATELLITE CHANNEL MODEL

During this work, the geosynchronous earth orbit (GEO) satellite is assumed. In addition, the satellite is considered to own several transmission beams. Moreover, time division multiple access (TDMA) [53] scheme is considered that leads to the result that only one terrestrial is used at each slot.

The channel coefficient $h_X, X \in \{\{SR\}, \{SE_j\}\}$ is represented as

$$h_X = C_X f_X, \tag{22}$$

where f_X denotes the random SR factor of the satellite channel, and C_X is the effect of antenna pattern and the free space loss (FSL), which can be written as

$$C_X = \frac{\lambda \sqrt{G_X G_{\text{Re}}}}{4\pi \sqrt{d^2 + d_0^2}}, \tag{23}$$

where λ denotes the wavelength of the frequency carrier, d represents the length from terrestrial relay/eavesdroppers to the satellite beam' center. $d_0 \approx 35786km$ is the antenna gain for terrestrial relay/eavesdroppers/monitors, furthermore, G_{Re} is the satellite on-board beam gain.

With the help of [20], G_{Re} can be approximated as

$$G_{Re}(dB) \simeq \begin{cases} \overline{G}_{\max}, & for\ 0^\circ < \vartheta < 1^\circ \\ 32 - 25\log\vartheta, & for\ 1^\circ < \vartheta < 48^\circ \\ -10, & for\ 48^\circ < \vartheta \le 180^\circ, \end{cases} \tag{24}$$

where $\overline{G}_{\max}$ represents the maximum beam gain, and ϑ denotes the off-boresight's angle. Considering G_X, by assuming θ_k being the angle, and $\bar{\theta}_k$ is regarded as the 3dB angle shown as [18], [22]

$$G_X \simeq G_{\max}\left(\frac{K_1(u_k)}{2u_k} + 36\frac{K_3(u_k)}{u_k^3}\right), \tag{25}$$

where G_{max} is the maximal beam gain, $u_k = 2.07123 \sin\theta_k / \sin\bar{\theta}_k$, K_1 and K_3 are the 1st-kind bessel function of order 1 and 3, respectively. To gain the best beam performance, $\theta_k \to 0$ is considered which leads to $G_X \approx G_{\max}$. Owing on this consideration, we get $h_X = C_X^{\max} f_X$.

For f_X, a popular SR model was mentioned in [54], which suits for land mobile satellite (LMS) systems [22]. By utilizing [54], the PDF of $\gamma_X = \overline{\gamma}_X |C_X^{\max} f_X|$ is obtained as

$$f_{\gamma_X}(x) = \alpha_X \sum_{k_X=0}^{m_X-1} \frac{(1-m_X)_{k_X}(-\delta_X)^{k_X}}{(k_X!)^2 \overline{\gamma}_X^{k_X+1}} x^{k_X} \exp(-\Delta_X x), \tag{26}$$

where $\overline{\gamma}_X$ denotes the average SNR from the satellite to terrestrial relay/eavesdroppers/monitors, $\Delta_X = \frac{\beta_X - \delta_X}{\overline{\gamma}_X}$, $\alpha_X = (\frac{2b_X m_X}{2b_X m_X + \Omega_X})^{m_X} / 2b_X$, $\beta_X = \frac{1}{2b_X}$, $\delta_X = \frac{\Omega_X}{2b_X(2b_X m_X + \Omega_X)}$, where $m_X \ge 0$ represents the fading severity parameter, $2b_Q$ denotes the multipath component's average power and Ω_X represents the line of sight (LoS) component's average power. Through this work, m_X is considered as an integer [14], [18], [22], when $m_X \to \infty$, the shadowed-Rician channel will be reduced to the Rician fading. $(\cdot)_{k_x}$ denotes the Pochhammer symbol [55].

Next, by utilizing (26), the CDF for γ_X is derived as

$$F_{\gamma_X}(x) = 1 - \sum_{k_X=0}^{m_X-1} \sum_{t=0}^{k_X} \frac{\alpha_X (1-m_X)_{k_X} (-\delta_X)^{k_X}}{t!(k_X!)\bar{\gamma}_X^{k_X+1} \Delta_X^{k_X-t+1}} x^t \exp(-\Delta_X x). \quad (27)$$

From [14], the PDF of γ_{SE} has the following expression as

$$f_{\gamma_{SE}}(x) = \sum_{k_{SE_1}=0}^{m_{SE}-1} \cdots \sum_{k_{SE_N}=0}^{m_{SE}-1} \Xi(N) x^{\Lambda-1} e^{-\Delta_{SE} x}, \quad (28)$$

where

$$\Xi(N) \triangleq \prod_{\tau=1}^{N} \xi(k_\tau) \alpha_{SE}^N \prod_{\upsilon=1}^{N-1} B\left(\sum_{l=1}^{\upsilon} k_l + \upsilon, k_{\upsilon+1} + 1\right),$$

$\Lambda \triangleq \sum_{\tau=1}^{N} k_\tau + N$, $\zeta(k_\tau) = \frac{(1-m_{SE})_{k_\tau}(-\delta_{SE})^{k_\tau}}{(k_\tau!)^2}$, $B(.,.)$ represents the Beta function [55].

2) THE TERRESTRIAL CHANNEL

As announced before, the channel coefficient between the relay and the ground users/eavesdroopers is considered to be shadowed as i.i.d Rayleigh fading. when colluding scheme is used at N monitors, the PDF of γ_V, $V \in (ED, RE)$ and γ_{RD} are, respectively, given by

$$f_{\gamma_V}(x) = \sum_{i=1}^{\rho(\mathrm{A}_V)} \sum_{j=1}^{\tau_i(\mathrm{A}_V)} \frac{\chi_{i,j}(\mathrm{A}_V)\bar{\gamma}_{\langle i \rangle}^{-j}}{(j-1)!} x^{j-1} e^{-\frac{x}{\bar{\gamma}_{\langle i \rangle}}}, \quad (29)$$

and

$$f_{\gamma_{RD}}(x) = \frac{1}{\overline{\gamma}_{RD}} e^{-\frac{x}{\bar{\gamma}_{RD}}}, \quad (30)$$

where $\mathrm{A}_V = \mathrm{diag}(\overline{\gamma}_1, \overline{\gamma}_2, \ldots, \overline{\gamma}_N)$, $\rho(\mathrm{A}_V)$ are the number of distinct diagonal elements of A_V, $\overline{\gamma}_{\langle 1 \rangle} > \overline{\gamma}_{\langle 2 \rangle} > \ldots > \overline{\gamma}_{\langle \rho(\mathrm{A}_V) \rangle}$ denote the distinct diagonal elements in decreasing order, $\tau_i(A_V)$ are the multiplicity of $\overline{\gamma}_{\langle i \rangle}$, and $\chi_{i,j}(\mathrm{A}_V)$ represents the (i,j)-th characteristic coefficient of A_V [56].

By utilizing (30), the CDF for γ_{RD} is written as

$$F_{\gamma_{RD}}(x) = 1 - e^{-\frac{x}{\bar{\gamma}_{RD}}}. \quad (31)$$

Besides, when $\bar{\gamma}_1 = \bar{\gamma}_2 =, \ldots, = \bar{\gamma}_V$, (29) can be written as

$$f_{\gamma_V}(x) = \frac{\bar{\gamma}_V^{-N}}{(N-1)!} x^{N-1} e^{-\frac{x}{\bar{\gamma}_V}}. \quad (32)$$

B. EAVESDROPPING NON-OUTAGE PROBABILITY

Based on [31] and [57], the ENOP is given by

$$P_{out} = \Pr\left(\gamma_E > \gamma_{F_q D}\right), q \in \{1, 2, 3\}. \quad (33)$$

The accurate expressions for the ENOP of the considered three cases are, respectively, given in the following.

1) CASE I: EAVESDROPPING THEN JAMMING

In this case, the ENOP is derived as

$$\begin{aligned} P_{out} &= \Pr\left(\gamma_E > \gamma_{F_1 D}\right), \\ &= \Pr\left(\gamma_E > \min\left(\gamma_{SR}, \gamma_{D_1}\right)\right) \\ &= \Pr\left[\gamma_E > \min\left(\gamma_{SR}, \frac{\gamma_{RD}}{\gamma_{ED}+1}\right)\right]. \end{aligned} \quad (34)$$

With the help of (34), this case can be observed as follows:

- If $\gamma_E > \gamma_{SR}$, it will satisfy that E can eavesdrop the signal successfully without any help, hence no more power is needed to jam the signal, namely $\gamma_{ED} = 0$ is set.
- If $\gamma_E < \gamma_{SR}$ and $\gamma_E > \gamma_{RD}$, E is also satisfied to overhear the signal successfully with no help, which also means γ_{ED} is set as 0.
- If $\gamma_E < \gamma_{SR}$ and $\gamma_{RD} > \gamma_E > \frac{\gamma_{RD}}{\gamma_{ED}+1}$, E can just its transmit power to maintain E can eavesdrop successfully.

Then, the final expressions for the ENOP is obtained in **Theorem 1**.

Theorem 1: The final expression for the ENOP in Case I is given by

$$\begin{aligned} P_{out} = &\sum_{k_{SE_1}=0}^{m_{SE}-1} \cdots \sum_{k_{SE_N}=0}^{m_{SE}-1} \sum_{k_{SR}=0}^{m_{SR}-1} \sum_{t=0}^{\Lambda-1} \Xi(N)\alpha_{SR} \\ &\times \frac{(1-m_{SR})_{k_{SR}}(-\delta_{SR})^{k_{SR}}(\Lambda-1)!}{(k_{SR}!)^2 \bar{\gamma}_{SR}^{k_{SR}+1} t! \Delta_{SE}^{\Lambda-t}} \\ &\times (k_{SR}+t)!(\Delta_{SE}+\Delta_{SR})^{-(k_{SR}+t+1)} \\ &+ \sum_{k_{SR}=0}^{m_{SR}-1} \sum_{k=0}^{k_{SR}} \frac{\alpha_{SR}(1-m_{SR})_{k_{SR}}(-\delta_{SR})^{k_{SR}}}{k! \Delta_{SR}^{k_{SR}-k+1} k_{SR}! \bar{\gamma}_{SR}^{k_{SR}+1}} \\ &\times \left[\sum_{k_{SE_1}=0}^{m_{SE}-1} \cdots \sum_{k_{SE_N}=0}^{m_{SE}-1} \frac{\Xi(N)(k+\Lambda-1)!}{(\Delta_{SE}+\Delta_{SR})^{k+\Lambda}} \right. \\ &- \sum_{i=1}^{\rho(\mathrm{A}_{ED})} \sum_{j=1}^{\tau_i(\mathrm{A}_{ED})} \frac{\chi_{i,j}(\mathrm{A}_{ED})\bar{\gamma}_{\langle i \rangle}^{-j}}{(j-1)!} \\ &\times \sum_{t=0}^{j-1} \Xi(N)(k+\Lambda-1)! \bar{\gamma}_{RD}^{k+\Lambda} \binom{n-1}{t} e^{\frac{A}{\bar{\gamma}_{\langle i \rangle}}} \\ &\left. \times (-A)^{j-1-t} H_3(-k-\Lambda+t, A, 1/\bar{\gamma}_{RD}) \right], \end{aligned} \quad (35)$$

where $A = 1 + (\Delta_{SE} + \Delta_{SR})\overline{\gamma}_{RD}$ and

$$H_3(n, b, u) = \begin{cases} H_1(n, b, u), n \geq 0 \\ H_2(-n-1, b, u), n < 0 \end{cases},$$

$$H_1(n, b, u) = e^{-bu} \sum_{k=0}^{n} \frac{n! b^k}{k! u^{n-k+1}},$$

and

$$H_2(n,b,u) = (-1)^{n+1}\frac{u^n Ei(-ub)}{n!} + \frac{e^{-ub}}{b^n}\sum_{k=0}^{n-1}\frac{(-bu)^k}{n(n-1)\cdots(n-k)}, \quad (36)$$

where $Ei(\cdot)$ denotes Exponential integral function [55, eq. (8).211.1].

Besides, when $\bar{\gamma}_1 = \bar{\gamma}_2 =, \ldots, = \bar{\gamma}_{ED}$, (35) can be written as

$$\begin{aligned} P_{out} &= \sum_{k_{SE_1}=0}^{m_{SE}-1}\cdots\sum_{k_{SE_N}=0}^{m_{SE}-1}\sum_{k_{SR}=0}^{m_{SR}-1}\sum_{t=0}^{\Lambda-1}\Xi(N)\alpha_{SR} \\ &\times \frac{(1-m_{SR})_{k_{SR}}(-\delta_{SR})^{k_{SR}}(\Lambda-1)!}{(k_{SR}!)^2\bar{\gamma}_{SR}^{k_{SR}+1}t!\Delta_{SE}^{\Lambda-t}} \\ &\times (k_{SR}+t)!(\Delta_{SE}+\Delta_{SR})^{-(k_{SR}+t+1)} \\ &+ \sum_{k_{SR}=0}^{m_{SR}-1}\sum_{k=0}^{k_{SR}}\frac{\alpha_{SR}(1-m_{SR})_{k_{SR}}(-\delta_{SR})^{k_{SR}}}{k!\Delta_{SR}^{k_{SR}-k+1}k_{SR}!\bar{\gamma}_{SR}^{k_{SR}+1}} \\ &\times \Bigg[\sum_{k_{SE_1}=0}^{m_{SE}-1}\cdots\sum_{k_{SE_N}=0}^{m_{SE}-1}\frac{\Xi(N)(k+\Lambda-1)!}{(\Delta_{SE}+\Delta_{SR})^{k+\Lambda}} \\ &- \frac{\bar{\gamma}_{ED}^{-N}}{(N-1)!}\sum_{t=0}^{N-1}\frac{\binom{n-1}{t}\Xi(N)(k+\Lambda-1)!}{\bar{\gamma}_{RD}^{-k-\Lambda}}e^{\frac{A}{\bar{\gamma}_{ED}}} \\ &\times (-A)^{N-1-t}H_3(-k-\Lambda+t, A, 1/\bar{\gamma}_{RD})\Bigg]. \quad (37) \end{aligned}$$

Proof: Please see Appendix A. ∎

2) CASE II: JAMMING THEN EAVESDROPPING

In this case, the ENOP is given by

$$\begin{aligned} P_{out} &= \Pr\big(\gamma_E > \gamma_{F_2D}\big) = \Pr\big(\gamma_E > \min\big(\gamma_{R_2}, \gamma_{D_2}\big)\big) \\ &= \Pr\left[\gamma_E > \min\left(\frac{\gamma_{SR}}{\gamma_{ER}+1}, \gamma_{RD}\right)\right]. \quad (38) \end{aligned}$$

From (38), this case can be analyzed in the following as

- If $\gamma_E > \gamma_{RD}$, it is sure that E could eavesdrop the signal successfully with no help, so we need not waste power to jam the signal, namely $\gamma_{ER} = 0$ is set.
- If $\gamma_E < \gamma_{RD}$ and $\gamma_E > \gamma_{SR}$, E is also satisfied to overhear the signal successfully with no help, which also means γ_{ER} is set as 0.
- If $\gamma_E < \gamma_{RD}$ and $\gamma_{SR} > \gamma_E > \frac{\gamma_{SR}}{\gamma_{ER}+1} = \frac{\gamma_{SR}}{\gamma_E P_{E_j}/P_R+1}$, E can just its transmit power to maintain E can eavesdrop successfully.

Then, the final expression for the ENOP is given in **Theorem 2**.

Theorem 2: The final expression for the ENOP in Case II is presented as

$$\begin{aligned} P_{out} &= \sum_{i=1}^{\rho(\mathrm{A}_{RE})}\sum_{j=1}^{\tau_i(\mathrm{A}_{RE})}\sum_{t=0}^{j-1}\frac{\chi_{i,j}(\mathrm{A}_{RE})\bar{\gamma}_{\langle i\rangle}^{-j}(\bar{\gamma}_{RE})^{j-t}}{\bar{\gamma}_{RD}(1/\bar{\gamma}_{RD}+1/\bar{\gamma}_{RE})^{t+1}} \\ &+ \sum_{k_{SR}=0}^{m_{SR}-1}\frac{\alpha_{SR}(1-m_{SR})_{k_{SR}}(-\delta_{SR})^{k_{SR}}}{k_{SR}!\bar{\gamma}_{SR}^{k_{SR}+1}\Delta_{SR}^{k_{SR}+1}} \\ &\times \sum_{i=1}^{\rho(\mathrm{A}_{RE})}\sum_{j=1}^{\tau_i(\mathrm{A}_{RE})}\chi_{i,j}(\mathrm{A}_{RE})\bar{\gamma}_{\langle i\rangle}^{-j}(1/\bar{\gamma}_{RD}+1/\bar{\gamma}_{RE})^{-j} \\ &- \sum_{k_{SR}=0}^{m_{SR}-1}\sum_{q=0}^{k_{SR}}\frac{\alpha_{SR}(1-m_{SR})_{k_{SR}}(-\delta_{SR})^{k_{SR}}}{q!\Delta_{SR}^{k_{SR}-1+q}k_{SR}!\bar{\gamma}_{SR}^{k_{SR}+1}} \\ &\times \sum_{v=0}^{q}\sum_{i=1}^{\rho(\mathrm{A}_{RE})}\sum_{j=1}^{\tau_i(\mathrm{A}_{RE})}\frac{\chi_{i,j}(\mathrm{A}_{RE})\bar{\gamma}_{\langle i\rangle}^{-j}\binom{q}{v}B^v}{(j-1)!} \\ &\times H_4(q+v+j-1, \Delta_{SR}B, 1/\bar{\gamma}_{RD}+1/\bar{\gamma}_{RE}+\Delta_{SR}), \end{aligned} \quad (39)$$

where

$$H_4(v,b,r) = (2b)^{-(v+1)/2}\Gamma(v+1)\exp\left(\frac{r^2}{8b}\right)D_{-v-1}\left(\frac{r}{\sqrt{2b}}\right), \quad (40)$$

$B = P_{E_j}/P_R$, $\Gamma(\cdot)$ denotes the Gamma Function [55, eq. (8).339.1], $D_v(\cdot)$ is the Parabolic cylinder functions [55, eq. (9).241.2].

Besides, when $\bar{\gamma}_1 = \bar{\gamma}_2 =, \ldots, = \bar{\gamma}_{RE}$, (39) can be written as

$$\begin{aligned} P_{out} &= \sum_{t=0}^{N-1}\frac{\bar{\gamma}_{RE}^{-t}}{\bar{\gamma}_{RD}(1/\bar{\gamma}_{RD}+1/\bar{\gamma}_{RE})^{t+1}} \\ &+ \sum_{k_{SR}=0}^{m_{SR}-1}\frac{\alpha_{SR}(1-m_{SR})_{k_{SR}}(-\delta_{SR})^{k_{SR}}}{k_{SR}!\bar{\gamma}_{SR}^{k_{SR}+1}\Delta_{SR}^{k_{SR}+1}\bar{\gamma}_{RE}^{N}(1/\bar{\gamma}_{RD}+1/\bar{\gamma}_{RE})^N} \\ &- \sum_{k_{SR}=0}^{m_{SR}-1}\sum_{q=0}^{k_{SR}}\sum_{v=0}^{q}\frac{\binom{q}{v}\bar{\gamma}_{RE}^{-N}B^v\alpha_{SR}(1-m_{SR})_{k_{SR}}(-\delta_{SR})^{k_{SR}}}{(N-1)!q!\Delta_{SR}^{k_{SR}-1+q}k_{SR}!\bar{\gamma}_{SR}^{k_{SR}+1}} \\ &\times H_4(q+v+j-1, \Delta_{SR}B, 1/\bar{\gamma}_{RD}+1/\bar{\gamma}_{RE}+\Delta_{SR}). \end{aligned} \quad (41)$$

Proof: Please see Appendix B. ∎

3) CASE III: ALWAYS EAVESDROPPING

In this case, the ENOP can be expressed as

$$\begin{aligned} P_{out} &= \Pr\big(\gamma_E > \gamma_{F_3D}\big) \\ &= \Pr\big[\gamma_{SE} + \gamma_{RE} > \min\big(\gamma_{R_3}, \gamma_{D_3}\big)\big]. \quad (42) \end{aligned}$$

Then, the final expression for the ENOP is given as **Theorem 3**.

Theorem 3: The final expression for the ENOP in Case III is given by

$$\begin{aligned} P_{out} &= 1 - \sum_{k_{SR}=0}^{m_{SR}-1}\sum_{t=0}^{k_{SR}}\sum_{k_{SE_1}=0}^{m_{SE}-1}\cdots\sum_{k_{SE_N}=0}^{m_{SE}-1}\sum_{i=1}^{\rho(\mathrm{A}_{RE})}\sum_{j=1}^{\tau_i(\mathrm{A}_{RE})}\Xi(N)\alpha_{SR} \\ &\times \frac{(1-m_{SR})_{k_{SR}}(-\delta_{SR})^{k_{SR}}\chi_{i,j}(\mathrm{A}_{RE})\bar{\gamma}_{\langle i\rangle}^{-j}}{t!(k_{SR}!)\bar{\gamma}_{SR}^{k_{SR}+1}\Delta_{SR}^{k_{SR}-t+1}(j-1)!} \end{aligned}$$

TABLE 2. Comparisons of three modes.

Cases	Case I	Case II	Case III
Advantages	ENOP can be controlled by jamming	ENOP can be controlled by jamming	Be found hard and invisibility
Disadvantages	Be found easily	Be found easily	ENOP can not be controlled

$$\times \sum_{v=0}^{t} \binom{t}{v} (v+\Lambda-1)!(\Delta_{SR}+1/\bar{\gamma}_{RD}+\Delta_{SE})^{-v-\Lambda} \times (t-v+j-1)!\left(\Delta_{SR}+1/\bar{\gamma}_{RD}+1/\bar{\gamma}_{\langle i\rangle}\right)^{-t+v-j}. \quad (43)$$

Besides, when $\bar{\gamma}_1 = \bar{\gamma}_2 =, \ldots, = \bar{\gamma}_{RE}$, (43) can be written as

$$P_{out} = 1 - \sum_{k_{SR}=0}^{m_{SR}-1} \sum_{t=0}^{k_{SR}} \sum_{k_{SE_1}=0}^{m_{SE}-1} \cdots \sum_{k_{SE_N}=0}^{m_{SE}-1} \frac{\Xi(N)\alpha_{SR}}{(N-1)!\bar{\gamma}_{RE}^{N}} \times \sum_{v=0}^{t} \binom{t}{v} \frac{\Delta_{SR}^{-k_{SR}+t-1}(1-m_{SR})_{k_{SR}}(-\delta_{SR})^{k_{SR}}(v+\Lambda-1)!}{t!(k_{SR}!)\bar{\gamma}_{SR}^{k_{SR}+1}\left(\Delta_{SR}+\frac{1}{\bar{\gamma}_{RD}}+\Delta_{SE}\right)^{v+\Lambda}} \times (t-v+N-1)!(\Delta_{SR}+1/\bar{\gamma}_{RD}+1/\bar{\gamma}_{RE})^{-t+v-N}. \quad (44)$$

Proof: See Appendix C. ■

C. ASYMPTOTIC ANALYSIS FOR ENOP

To derive further investigations on the system performance, in this subsection, the asymptotic analysis for the ENOP of three cases will given in the following. For the convenience, we assume that $\bar{\gamma}_{RD} = \bar{\gamma}_{SR} = \bar{\gamma}$. So, when $\bar{\gamma} \to \infty$, namely $1/\bar{\gamma} \to 0$.

For Case I in (35), $Ei(x)$ can be re-written as

$$Ei(x) = \sigma + \ln x + \sum_{k=1}^{\infty} \frac{x^k}{k!k}, \quad (45)$$

where $\sigma = 0.57721566$ is Euler-Mascheroni constant.

During high SNR regimes, in this paper which means $x \to 0$, then the high order components of the series can be omitted, thus we can get the asymptotic expression of (45) as

$$\underset{x\to 0}{Ei(x)} = \sigma + \ln x + x + o(x), \quad (46)$$

where $o(x)$ represents the higher order of x.

By substituting (46) into (35), the asymptotic expression of ENOP for Case I can be obtained.

For Case II, with the similar method, when at high SNRs which means $z \to 0$ in this paper, by utilizing the [55], we derive

$$\underset{z\to 0}{D_p(z)} = e^{-z^2/4} z^p \left[1 - \frac{p(p-1)}{2z^2}\right] + o(z). \quad (47)$$

The asymptotic ENOP of Case II can be obtained by taking (47) into (39).

For Case III, we attempt to use a different way to calculate the asymptotic analysis, when $\bar{\gamma}_{SR} = \bar{\gamma}_{RD} = \bar{\gamma} \to \infty$, (27) and (31) can be re-written as

$$F_{\gamma_{SR}}(x) = \frac{\alpha_{SR} x}{\bar{\gamma}_{SR}} + o(x), \quad (48)$$

TABLE 3. Channel parameters.

Shadowing	m_X	b_X	Ω_X
Frequent heavy shadowing (FHS) [14]	1	0.063	0.0007
Average shadowing (AS) [14]	5	0.251	0.279
Infrequent light shadowing (ILS) [14]	10	0.158	1.29

TABLE 4. System parameters.

Parameters	Value
Satellite Orbit	GEO [18]
Frequency band	$f = 2$ GHz [18]
Maximal Beam Gain	$G_{max} = 48$ dB [18]
The Antenna Gain	$G_{Re} = 4$ dB [18]

and

$$F_{\gamma_{RD}}(x) = \frac{x}{\bar{\gamma}_{RD}} + o(x). \quad (49)$$

Then, by substituting (48) and (49) into the derivation of **Theorem 3** and utilizing the same method, after some mathematical steps, the asymptotic expression will be derived as

$$P_{out}^{\infty} = \sum_{k_{SE_1}=0}^{m_{SE}-1} \cdots \sum_{k_{SE_N}=0}^{m_{SE}-1} \sum_{i=1}^{\rho(\mathrm{A}_{RE})} \sum_{j=1}^{\tau_i(\mathrm{A}_{RE})} \frac{\alpha_{SR}\Xi(N)\chi_{i,j}(\mathrm{A}_{RE})}{(j-1)!\bar{\gamma}_{\langle i\rangle}^{j+N+1}\Delta_{SE}^{\Lambda+1}} \times \frac{(\alpha_{SR}+1)(j-1)!}{\bar{\gamma}[(\Lambda)!]^{-1}} - \sum_{k_{SE_1}=0}^{m_{SE}-1} \cdots \sum_{k_{SE_N}=0}^{m_{SE}-1} \sum_{i=1}^{\rho(\mathrm{A}_{RE})} \sum_{j=1}^{\tau_i(\mathrm{A}_{RE})} \alpha_{SR} \times \sum_{v=0}^{2} \binom{2}{v} \frac{\Xi(N)\chi_{i,j}(\mathrm{A}_{RE})(v+\Lambda-1)!(j-v)!}{(j-1)!(\bar{\gamma})^2\Delta_{SE}^{v+\Lambda}\bar{\gamma}_{\langle i\rangle}^{-(1-v+N-j)}}. \quad (50)$$

From the former analysis, we summarize the advantages and disadvantages of the three modes in TABLE 2, which shown at the top of next page.

IV. NUMERICAL RESULTS

Analytical analysis is verified by the several simulations below in this Section. In general, we assume the GEO satellite,[7] and $\delta_R^2 = \delta_D^2 = \delta_{E_j}^2 = 1$, $\bar{\gamma}_{SR} = \bar{\gamma}_{RD} = \bar{\gamma} = 20dB$ for Case I and Case II, besides, $\bar{\gamma}_{SE} = \bar{\gamma}_{RE} = \bar{\gamma}_E$. The channel and system parameters of satellite-terrestrial channel are provided in Table 3 [14] and Table 4 [18], respectively.[8]

From the simulation figures, we can easily get that our theoretical solutions are well consistent with MC simulations, which means that the correctness of our theoretical derivation has been proved. Besides, in high SNR regime, it can be clearly found that the asymptotic investigations are in line with theoretical analysis, which verifies the effectiveness of our asymptotic results.

7. Although in this paper GEO satellite is assumed, our derivations are still for the cases for medium earth orbit (MEO) satellite and low earth orbit (LEO) satellite.

8. Although in this paper, these assumptions are set, the other assumptions will be investigated in our near future. The derived results will give some guidance for the future analysis.

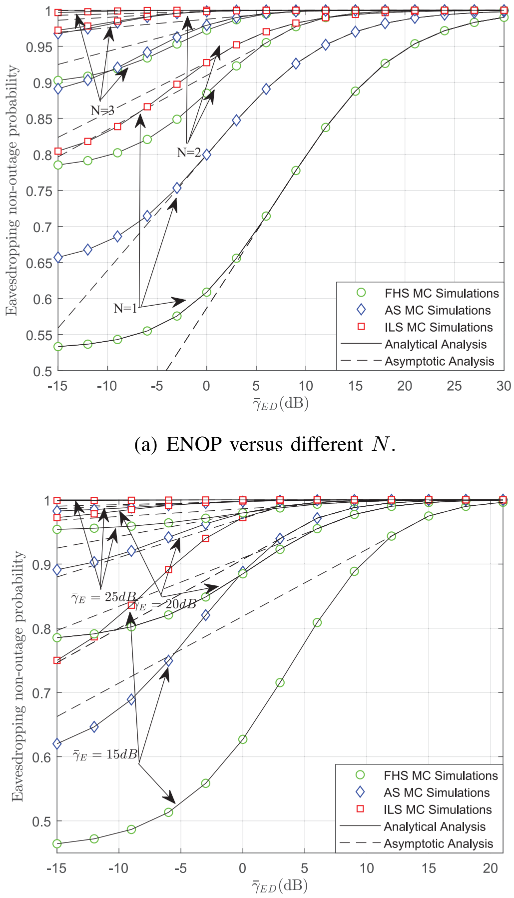

(a) ENOP versus different N.

(b) ENOP versus different $\overline{\gamma}_E$.

FIGURE 2. **ENOP of Case I.**

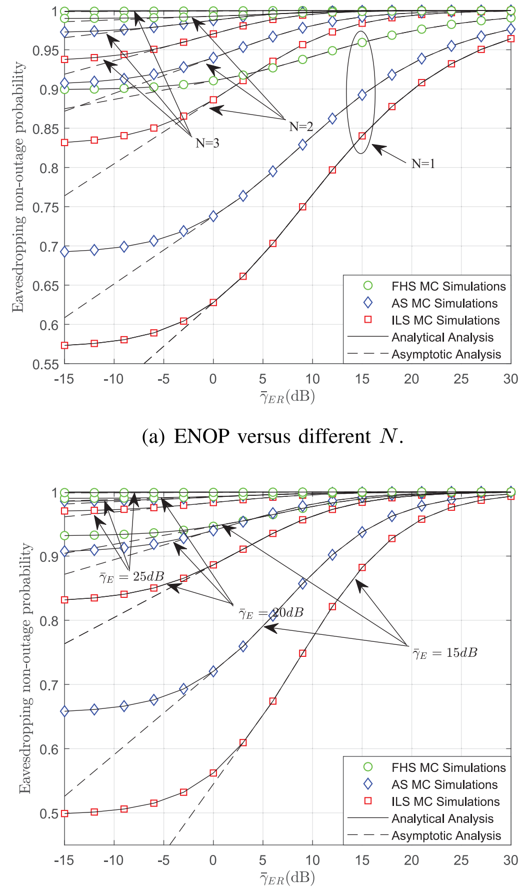

(a) ENOP versus different N.

(b) ENOP versus different $\overline{\gamma}_E$.

FIGURE 3. **ENOP of Case II.**

Fig. 2(a) illustrates the ENOP of Case I versus different N with $\overline{\gamma}_E = 20dB$. It can be clearly observed that the active eavesdropping performance of the system improves with the numbers of monitors increasing, which verifies the superiority of our considered scheme. Furthermore, ENOP is higher under favorable satellite-terrestrial channel conditions, which shows that the better channel condition bring better eavesdropping performance. In addition, when $\overline{\gamma}_{ED}$ increases, the jamming will interference the users easier. Moreover, we find that when N increases, the ENOP will be larger for the reason that more monitors work together to jam or overhear the legitimate signals.

Fig. 2(b) shows that the ENOP of Case I versus different $\overline{\gamma}_E$ with setting $N = 2$. We can find that the ENOP enhances as the $\overline{\gamma}_E$ increases. This is because the larger $\overline{\gamma}_E$ will enhance the jamming or eavesdropping ability.

Both from Fig. 2(a) and Fig. 2(b), when the power of monitors becomes larger enough, the ENOP will be always 1, which is the inherent character of the proactive eavesdropping scenario.

Fig. 3(a) depicts the ENOP of Case II versus different N with $\overline{\gamma}_E = 20dB$. It can be found that ENOP increases with the enhancement of N as well as $\overline{\gamma}_{ER}$, which is similar to the results of Case I. However, an improved system performance is obtained with worse channel condition of SR fading, which is opposite of case I. The reason can be explained by the fact that monitors improve eavesdropping performance by interfering the relay in Case II. However, when the system is under light channel fading, the ENOP will be lower, which means the channel fading has great impact on the system performance. Fig. 3(b) plots the ENOP of Case II versus different $\overline{\gamma}_E$. Similar to Case I, the degradation of $\overline{\gamma}_E$ will lead to the deterioration of ENOP. The similar conclusion with Fig. 2(a), when N increases, the ENOP will be larger for the reason that more monitors join to jam or overhear the legitimate signals.

The similar results with Fig. 2, in Fig. 3, when the power of monitors becomes larger enough, the ENOP will be always 1, which is caused by the proactive scenario.

Fig. 4(a) examines the ENOP of Case III for the system with $\bar{\gamma}_E$=6dB. It should be pointed out that the simulation settings of Fig. 4 is different from that of Fig. 2 or Fig. 3. In this figure, $\bar{\gamma}$ is not fixed, it is shown as the abscissa varying from 0 to 40dB. This is very different from the former simulation settings. From Fig. 4(a), we can derive that when the number of eavesdroppers grows larger, the ENOP would be larger, which means the eavesdropping will be interrupted at a high probability. Finally, we can derive that the light channel fading brings a lower ENOP.

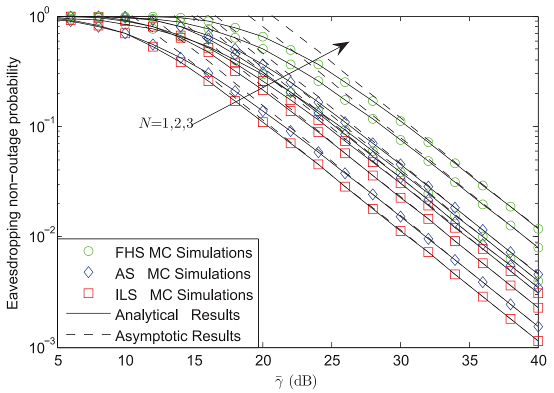

(a) ENOP versus different N.

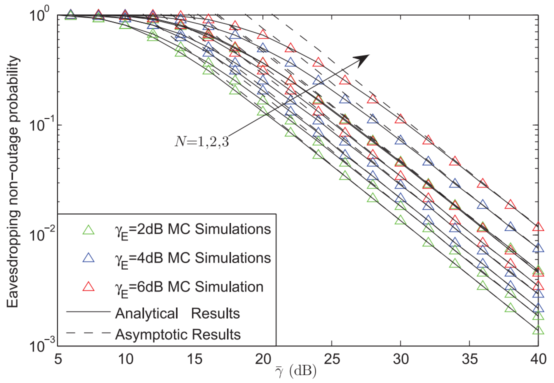

(b) ENOP versus different $\overline{\gamma}_E$.

FIGURE 4. ENOP of Case III.

Fig. 4(b) illustrates the ENOP of Case III for the system with different $\bar{\gamma}_E$ with FHS scenario. The insightful results from this figure is that a larger $\bar{\gamma}_E$ brings a larger ENOP. Both from Fig. 4(a) and Fig. 4(b), the interesting thing is that, the ENOP will be lower when the transmitted power for the legitimate link grows larger, which results from the reason that when the legitimate link's power grows larger, the performance for the legitimate links is enhanced, it is hard to overhear the legitimate link. It is not hard to understand that when the power for the eavesdroppers becomes larger, the performance for the eavesdropper will be better in a reasonable manner.

Fig. 5 examines the ENOP versus different $\bar{\gamma}_{ED}$ or $\bar{\gamma}_{ER}$ for three Cases with $\bar{\gamma}$=20dB, N=2 and $\bar{\gamma}_E$=15dB in ILS scenario. From Fig. 5, we can find that when ($\bar{\gamma}_{ED}$ or $\bar{\gamma}_{ER}$) is smaller than a fixed value, Case III has the largest ENOP, however, when ($\bar{\gamma}_{ED}$ or $\bar{\gamma}_{ER}$) is larger than this value, Case II will gain the largest ENOP, which will guide us how to allocate ($\bar{\gamma}_{ED}$ or $\bar{\gamma}_{ER}$) to have the largest ENOP, which has the same phenomenon as [58]. In Fig. 5, we can also find that when all the simulation settings are the same, the ENOP for Case III will be a constant, which is not affected by $\bar{\gamma}_{ED}$ or $\bar{\gamma}_{ER}$. This is because, jamming does not exist in Case III.

V. CONCLUSION

Through this paper, the proactive eavesdropping based legitimate surveillance in ISTRNs with multiple monitors

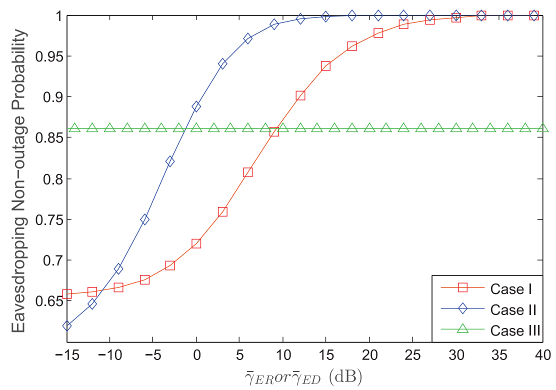

FIGURE 5. ENOP versus different $\bar{\gamma}_{ED}$ or $\bar{\gamma}_{ER}$ for three Cases with $\bar{\gamma}$=20dB, N=2, and $\bar{\gamma}_E$=15dB in ILS scenario.

was investigated. Specifically, three proactive eavesdropping modes were proposed in our paper, besides, the theoretical and asymptotic analysis of ENOP for the three cases were further, respectively, derived. The numerical results indicated the characters of the three proactive eavesdropping cases. In addition, the impacts of major system and channel parameters were investigated on the considered system. The results showed that the power for the legitimate users, the power of the monitors, the number of the monitors, and the channel fading had serious impacts on the proactive eavesdropping performance.

APPENDIX A
PROOF OF THEOREM 1

From (34), the P_{out} is given by

$$P_{out} = \underbrace{\Pr(\gamma_{SE} \geq \gamma_{SR})}_{C_{11}} + \underbrace{\Pr\left(\gamma_{SR} > \gamma_{SE} > \frac{\gamma_{RD}}{\gamma_{ED}+1}\right)}_{C_{12}}. \quad (51)$$

From (51), the important thing is to derive C_{11} and C_{12}, the detailed steps are shown in the following.

Firstly, by utilizing (51), C_{11} can be written as

$$C_{11} = \int_0^{\infty}\int_y^{\infty} f_{\gamma_{SE}}(x) f_{\gamma_{SR}}(y)\,dx\,dy. \quad (52)$$

By taking (26) with $X = SR$ and (28) into (52), with the utilizing of [55, eq. (3).351.2], (52) can be rewritten as

$$C_{11} = \sum_{k_{SE_1}=0}^{m_{SE}-1}\cdots\sum_{k_{SE_N}=0}^{m_{SE}-1}\sum_{k_{SR}=0}^{m_{SR}-1}\sum_{t=0}^{\Lambda-1}\Xi(N)\alpha_{SR} \times\frac{(1-m_{SR})_{k_{SR}}(-\delta_{SR})^{k_{SR}}(\Lambda-1)!}{(k_{SR}!)^2\bar{\gamma}_{SR}^{k_{SR}+1}t!\Delta_{SE}^{\Lambda-t}}\int_0^{\infty} y^{k_{SR}+t}e^{-(\Delta_{SE}+\Delta_{SR})y}dy. \quad (53)$$

Next, by using [55, eq. (3).351.1], (53) is finally derived as

$$C_{11} = \sum_{k_{SE_1}=0}^{m_{SE}-1}\cdots\sum_{k_{SE_N}=0}^{m_{SE}-1}\sum_{k_{SR}=0}^{m_{SR}-1}\sum_{t=0}^{\Lambda-1}\Xi(N)(k_{SR}+t)! \times\frac{\alpha_{SR}(1-m_{SR})_{k_{SR}}(-\delta_{SR})^{k_{SR}}(\Lambda-1)!}{(k_{SR}!)^2\bar{\gamma}_{SR}^{k_{SR}+1}t!\Delta_{SE}^{\Lambda-t}(\Delta_{SE}+\Delta_{SR})^{k_{SR}+t+1}}. \quad (54)$$

Secondly, with the help of (51), the second part C_{12} is expressed as

$$C_{12} = \int_0^\infty \int_0^\infty \int_0^{zp+z} \int_z^\infty f_{\gamma_{SR}}(x) f_{\gamma_{RD}}(y) \times f_{\gamma_{SE}}(z) f_{\gamma_{ED}}(p) dxdydzdp. \quad (55)$$

Then, by inserting (26) with $X = SR$ into (55) and with the help of [55, eq. (3).351.2], (55) can be re-written as

$$C_{12} = \int_0^\infty \int_0^\infty \int_0^{zp+z} f_{\gamma_{RD}}(y) f_{\gamma_{SE}}(z) f_{\gamma_{ED}}(p) \times \sum_{k_{SR}=0}^{m_{SR}-1} \sum_{k=0}^{k_{SR}} \frac{\alpha_{SR}(1-m_{SR})_{k_{SR}}(-\delta_{SR})^{k_{SR}}}{k!\Delta_{SR}^{k_{SR}-k+1} k_{SR}! \bar{\gamma}_{SR}^{k_{SR}+1}} z^k e^{-\Delta_{SR} z} dydzdp. \quad (56)$$

After that, with the help of (30), (56) can be rewritten as

$$C_{12} = \int_0^\infty \int_0^\infty \sum_{k_{SR}=0}^{m_{SR}-1} \sum_{k=0}^{k_{SR}} \frac{\alpha_{SR}(1-m_{SR})_{k_{SR}}(-\delta_{SR})^{k_{SR}}}{k!\Delta_{SR}^{k_{SR}-k+1} k_{SR}! \bar{\gamma}_{SR}^{k_{SR}+1}} \times f_{\gamma_{SE}}(z) f_{\gamma_{ED}}(p) z^k e^{-\Delta_{SR} z} dzdp - \int_0^\infty \int_0^\infty \sum_{k_{SR}=0}^{m_{SR}-1} \sum_{k=0}^{k_{SR}} \frac{\alpha_{SR}(1-m_{SR})_{k_{SR}}(-\delta_{SR})^{k_{SR}}}{k!\Delta_{SR}^{k_{SR}-k+1} k_{SR}! \bar{\gamma}_{SR}^{k_{SR}+1}} \times f_{\gamma_{SE}}(z) f_{\gamma_{ED}}(p) z^k e^{-\Delta_{SR} z} e^{-\frac{zp+z}{\bar{\gamma}_{RD}}} dzdp. \quad (57)$$

By taking (28) and (29) into (57), and with the help of [55, eq.(111, 3.351.3)], (57) is finally obtained as

$$C_{12} = \sum_{k_{SR}=0}^{m_{SR}-1} \sum_{k=0}^{k_{SR}} \frac{\alpha_{SR}(1-m_{SR})_{k_{SR}}(-\delta_{SR})^{k_{SR}}}{k!\Delta_{SR}^{k_{SR}-k+1} k_{SR}! \bar{\gamma}_{SR}^{k_{SR}+1}} \times \sum_{k_{SE_1}=0}^{m_{SE}-1} \cdots \sum_{k_{SE_N}=0}^{m_{SE}-1} \frac{\Xi(N)(k+\Lambda-1)!}{(\Delta_{SE}+\Delta_{SR})^{k+\Lambda}} - \sum_{k_{SR}=0}^{m_{SR}-1} \sum_{k=0}^{k_{SR}} \frac{\alpha_{SR}(1-m_{SR})_{k_{SR}}(-\delta_{SR})^{k_{SR}}}{k!\Delta_{SR}^{k_{SR}-k+1} k_{SR}! \bar{\gamma}_{SR}^{k_{SR}+1}} \times \sum_{k_{SE_1}=0}^{m_{SE}-1} \cdots \sum_{k_{SE_N}=0}^{m_{SE}-1} \Xi(N) \sum_{i=1}^{\rho(\mathrm{A}_{ED})} \sum_{j=1}^{\tau_i(\mathrm{A}_{ED})} \frac{\chi_{i,j}(\mathrm{A}_{ED}) \bar{\gamma}_{\langle i \rangle}^{-j}}{(j-1)!} \times (k+\Lambda-1)! \bar{\gamma}_{RD}^{k+\Lambda} \int_0^\infty (A+p)^{-(k+\Lambda)} p^{j-1} e^{-\frac{p}{\bar{\gamma}_{\langle i \rangle}}} dp. \quad (58)$$

By utilizing [55, eq. (3).351.3] and (55), C_{12} can be obtained as

$$C_{12} = \sum_{k_{SR}=0}^{m_{SR}-1} \sum_{k=0}^{k_{SR}} \frac{\alpha_{SR}(1-m_{SR})_{k_{SR}}(-\delta_{SR})^{k_{SR}}}{k!\Delta_{SR}^{k_{SR}-k+1} k_{SR}! \bar{\gamma}_{SR}^{k_{SR}+1}} \times \Bigg[\sum_{k_{SE_1}=0}^{m_{SE}-1} \cdots \sum_{k_{SE_N}=0}^{m_{SE}-1} \frac{\Xi(N)(k+\Lambda-1)!}{(\Delta_{SE}+\Delta_{SR})^{k+\Lambda}} - \sum_{i=1}^{\rho(\mathrm{A}_{ED})} \sum_{j=1}^{\tau_i(\mathrm{A}_{ED})} \frac{\chi_{i,j}(\mathrm{A}_{ED}) \bar{\gamma}_{\langle i \rangle}^{-j}}{(j-1)!} \times \sum_{t=0}^{j-1} \Xi(N)(k+\Lambda-1)! \bar{\gamma}_{RD}^{k+\Lambda} \binom{n-1}{t} e^{\frac{A}{\bar{\gamma}_{\langle i \rangle}}} \times (-A)^{j-1-t} H_3(-k-\Lambda+t, A, 1/\bar{\gamma}_{RD}) \Bigg]. \quad (59)$$

At last, by taking (54) and (59) into (51), (35) will be derived.

For the scenario with $\bar{\gamma}_1 = \bar{\gamma}_2 =, \ldots, = \bar{\gamma}_{ED}$, by replacing (29) with (32), then with the similar method of the former presentations, (37) will be obtained, the final expression for ENOP in Case II can be derived.

The proof of **Theorem 1** is over.

APPENDIX B
PROOF OF THEOREM 2

Similar to Appendix A, P_{out} is re-written as

$$P_{out} = \underbrace{\Pr(\gamma_{RE} \geq \gamma_{RD})}_{C_{21}} + \underbrace{\Pr\left(\gamma_{RD} > \gamma_{RE} > \frac{\gamma_{SR}}{\gamma_{RE}+1}\right)}_{C_{22}}, \quad (60)$$

where

$$C_{21} = \int_0^\infty \int_y^\infty f_{\gamma_{RE}}(x) f_{\gamma_{RD}}(y) dxdy. \quad (61)$$

By taking (29) and (30) into (61) and with the utilization of [55, eq.351.2, 3.351.3], (61) is re-written as

$$C_{21} = \sum_{i=1}^{\rho(\mathrm{A}_{RE})} \sum_{j=1}^{\tau_i(\mathrm{A}_{RE})} \sum_{t=0}^{j-1} \frac{\chi_{i,j}(\mathrm{A}_{RE}) \bar{\gamma}_{\langle i \rangle}^{-j} (\bar{\gamma}_{RE})^{j-t}}{\bar{\gamma}_{RD}(1/\bar{\gamma}_{RD} + 1/\bar{\gamma}_{RE})^{t+1}}. \quad (62)$$

Besides, the second item C_{22} is given by

$$C_{22} = \int_0^\infty \int_0^{Bz^2+z} \int_z^\infty f_{\gamma_{RD}}(x) f_{\gamma_{SR}}(y) f_{\gamma_{RE}}(z) dxdydz. \quad (63)$$

Then, by substituting (30) into (63), we can obtain

$$C_{22} = \int_0^\infty \int_0^{Bz^2+z} f_{\gamma_{SR}}(y) f_{\gamma_{RE}}(z) e^{-\frac{z}{\bar{\gamma}_{RD}}} dydz. \quad (64)$$

By utilizing (26) and [55, Eqs. 111, 3.351.1, 3.351.3], (64) can be rewritten as

$$C_{22} = \sum_{k_{SR}=0}^{m_{SR}-1} \sum_{i=1}^{\rho(\mathrm{A}_{RE})} \sum_{j=1}^{\tau_i(\mathrm{A}_{RE})} \frac{\alpha_{SR}(1-m_{SR})_{k_{SR}}(-\delta_{SR})^{k_{SR}}}{k_{SR}! \bar{\gamma}_{SR}^{k_{SR}+1} \Delta_{SR}^{k_{SR}+1}} \times \chi_{i,j}(\mathrm{A}_{RE}) \bar{\gamma}_{\langle i \rangle}^{-j} (1/\bar{\gamma}_{RD} + 1/\bar{\gamma}_{RE})^{-j} - \sum_{k_{SR}=0}^{m_{SR}-1} \sum_{q=0}^{k_{SR}} \sum_{v=0}^{q} \sum_{i=1}^{\rho(\mathrm{A}_{RE})} \sum_{j=1}^{\tau_i(\mathrm{A}_{RE})} \frac{\alpha_{SR}(1-m_{SR})_{k_{SR}}}{q!\Delta_{SR}^{k_{SR}-1+q}} \times \frac{(-\delta_{SR})^{k_{SR}} \chi_{i,j}(\mathrm{A}_{RE}) \bar{\gamma}_{\langle i \rangle}^{-j} \binom{q}{v} B^v}{k_{SR}! \bar{\gamma}_{SR}^{k_{SR}+1} (j-1)!} \times \int_0^\infty z^{j+q+v-1} e^{-\left(\frac{1}{\bar{\gamma}_{RD}} + \frac{1}{\bar{\gamma}_{RE}} + \Delta_{SR}\right) z - B\Delta_{SR} z^2} dz. \quad (65)$$

After that, by taking (29) into (65) and with the help of [55, eq. (3).462.1], C_{22} is finally obtained as

$$C_{22} = \sum_{k_{SR}=0}^{m_{SR}-1} \sum_{i=1}^{\rho(A_{RE})} \sum_{j=1}^{\tau_i(A_{RE})} \frac{\alpha_{SR}(1-m_{SR})_{k_{SR}}(-\delta_{SR})^{k_{SR}}}{k_{SR}!\bar{\gamma}_{SR}^{k_{SR}+1}\Delta_{SR}^{k_{SR}+1}} \times \chi_{i,j}(A_{RE})\bar{\gamma}_{\langle i\rangle}^{-j}(1/\bar{\gamma}_{RD}+1/\bar{\gamma}_{RE})^{-j} - \sum_{k_{SR}=0}^{m_{SR}-1}\sum_{q=0}^{k_{SR}}\sum_{v=0}^{q}\sum_{i=1}^{\rho(A_{RE})}\sum_{j=1}^{\tau_i(A_{RE})} \frac{\alpha_{SR}(1-m_{SR})_{k_{SR}}}{q!\Delta_{SR}^{k_{SR}-1+q}} \times \frac{(-\delta_{SR})^{k_{SR}}\chi_{i,j}(A_{RE})\bar{\gamma}_{\langle i\rangle}^{-j}\binom{q}{v}B^v}{k_{SR}!\bar{\gamma}_{SR}^{k_{SR}+1}(j-1)!} \times H_4(q+v+j-1, \Delta_{SR}B, 1/\bar{\gamma}_{RD}+1/\bar{\gamma}_{RE}+\Delta_{SR}). \tag{66}$$

At last, by substituting (62) and (66) into (60), (39) will be obtained, the final expression for ENOP in Case II can be derived.

For the scenario with $\bar{\gamma}_1 = \bar{\gamma}_2 =, \ldots, = \bar{\gamma}_{RE}$, by replacing (29) with (32), then with the similar method of the former presentations, (39) will be obtained.

The proof of **Theorem 2** is gotten.

APPENDIX C
PROOF OF THEOREM 3

Recalling (42), (42) is written as

$$P_{out} = \Pr[\gamma_{SE}+\gamma_{RE} > \min(\gamma_{R_3}, \gamma_{D_3})] = \Pr[\min(\gamma_{R_3}, \gamma_{D_3}) < \gamma_{SE}+\gamma_{RE}] = \int_0^\infty\int_0^\infty\int_0^{x+y} f_{\gamma_{F_3D}}(z) f_{\gamma_{SE}}(x) f_{\gamma_{RE}}(y)\,dz\,dx\,dy. \tag{67}$$

From (67), we can get the first thing is to obtain the CDF for $F_{\gamma_{F_3D}}(z)$. By utilizing (20), the CDF for γ_{F_3D} is given by

$$F_{\gamma_{F_3D}}(x) = F_{\gamma_{R_3}}(x) + F_{\gamma_{D_3}}(x) - F_{\gamma_{R_3}}(x)F_{\gamma_{D_3}}(x). \tag{68}$$

By inserting (16) and (18) into (68), (68) is written as

$$F_{\gamma_{F_3D}}(x) = F_{\gamma_{SR}}(x) + F_{\gamma_{RD}}(x) - F_{\gamma_{SR}}(x)F_{\gamma_{RD}}(x). \tag{69}$$

Next, by substituting (27) and (31) into (69), (69) is given by

$$F_{\gamma_{F_3D}}(x) = 1 - \sum_{k_{SR}=0}^{m_{SR}-1}\sum_{t=0}^{k_{SR}} \frac{\alpha_{SR}(1-m_{SR})_{k_{SR}}(-\delta_{SR})^{k_{SR}}x^t}{t!(k_{SR}!)\bar{\gamma}_{SR}^{k_{SR}+1}\Delta_{SR}^{k_{SR}-t+1}} \times \exp[-(1/\bar{\gamma}_{RD}+\Delta_{SR})x]. \tag{70}$$

Then, by inserting (70) into (67), (67) can be written as

$$P_{out} = 1 - \sum_{k_{SR}=0}^{m_{SR}-1}\sum_{t=0}^{k_{SR}} \frac{\alpha_{SR}(1-m_{SR})_{k_{SR}}(-\delta_{SR})^{k_{SR}}}{t!(k_{SR}!)\bar{\gamma}_{SR}^{k_{SR}+1}\Delta_{SR}^{k_{SR}-t+1}} \int_0^\infty\int_0^\infty (x+y)^t \times \exp[-(1/\bar{\gamma}_{RD}+\Delta_{SR})(x+y)] f_{\gamma_{SE}}(x) f_{\gamma_{RE}}(y)\,dx\,dy$$
$$= 1 - \sum_{k_{SR}=0}^{m_{SR}-1}\sum_{t=0}^{k_{SR}} \frac{\alpha_{SR}(1-m_{SR})_{k_{SR}}(-\delta_{SR})^{k_{SR}}}{t!(k_{SR}!)\bar{\gamma}_{SR}^{k_{SR}+1}\Delta_{SR}^{k_{SR}-t+1}} \sum_{v=0}^{t}\binom{t}{v} \times \underbrace{\int_0^\infty x^v \exp[-(1/\bar{\gamma}_{RD}+\Delta_{SR})x] f_{\gamma_{SE}}(x)\,dx}_{C_{31}} \times \underbrace{\int_0^\infty \exp[-(1/\bar{\gamma}_{RD}+\Delta_{SR})y] y^{t-v} f_{\gamma_{RE}}(y)\,dx\,dy}_{C_{32}}. \tag{71}$$

Then, by substituting (28) with $X = SE$ into C_{31}, C_{31} can be obtained as

$$C_{31} = \sum_{k_{SE_1}=0}^{m_{SE}-1}\cdots\sum_{k_{SE_N}=0}^{m_{SE}-1} \Xi(N) \times \int_0^\infty x^{v+\Lambda-1}\exp[-(1/\bar{\gamma}_{RD}+\Delta_{SR}+\Delta_{SE})x]dx. \tag{72}$$

Next, with the help of [55, eq. (3.351.3)], C_{31} can be re-given as

$$C_{31} = \sum_{k_{SE_1}=0}^{m_{SE}-1}\cdots\sum_{k_{SE_N}=0}^{m_{SE}-1} \frac{\Xi(N)(v+\Lambda-1)!}{(1/\bar{\gamma}_{RD}+\Delta_{SR}+\Delta_{SE})^{v+\Lambda}}. \tag{73}$$

With the similar method, by inserting (29) with $V = RE$ into C_{32}, C_{32} can be re-represented as

$$C_{32} = \sum_{i=1}^{\rho(A_{RE})}\sum_{j=1}^{\tau_i(A_{RE})} \frac{\chi_{i,j}(A_{RE})\bar{\gamma}_{\langle i\rangle}^{-j}(t-v+j-1)!}{(j-1)!(1/\bar{\gamma}_{RD}+\Delta_{SR}+1/\bar{\gamma}_{\langle i\rangle})^{t-v+j}}. \tag{74}$$

At last, by taking (73) and (74) into (71), the final expression for ENOP in Case III can be derived.

For the scenario with $\bar{\gamma}_1 = \bar{\gamma}_2 =, \ldots, = \bar{\gamma}_{RE}$, by replacing (29) with (32), then with the similar method of the former presentations, (44) will be obtained.

The proof of **Theorem 3** is over.

REFERENCES

[1] O. Kodheli et al., "Satellite communications in the new space era: A survey and future challenges," *IEEE Commun. Surveys Tuts.*, vol. 23, no. 1, pp. 70–109, 1st Quart., 2021.

[2] X. Yue et al., "Outage behaviors of NOMA-based satellite network over shadowed-Rician fading channel," *IEEE Trans. Veh. Technol.*, vol. 69, no. 6, pp. 6818–6821, Jun. 2020.

[3] K. Guo, M. Wu, X. Li, H. Song, and N. Kumar, "Deep reinforcement learning and NOMA-based multi-objective RIS-assisted IS-UAV-TNs: Trajectory optimization and beamforming design," *IEEE Trans. Intell. Transp. Syst.*, vol. 24, no. 9, pp. 10197–10210, Sep. 2023.

[4] X. Lin, H. Zhang, G. Pan, S. Wang, and J. An, "LEO relay-aided GEO satellite-terrestrial transmission," *IEEE Trans. Veh. Technol.*, early access, Jul. 31, 2023, doi: 10.1109/TVT.2023.3299964.

[5] B. Li, Z. Fei, C. Zhou, and Y. Zhang, "Physical-layer security in space information networks: A survey," *IEEE Internet Things J.*, vol. 7, no. 1, pp. 33–52, Jan. 2020.

[6] K. Guo, M. Lin, B. Zhang, W.-P. Zhu, J.-B. Wang, and T. A. Tsiftsis, "On the performance of LMS communication with hardware impairments and interference," *IEEE Trans. Commun.*, vol. 67, no. 2, pp. 1490–1505, Feb. 2019.

[7] G. Pan, H. Zhang, R. Zhang, S. Wang, J. An, and M.-S. Alouini, "Space simultaneous information and power transfer: An enhanced technology for miniaturized satellite systems," *IEEE Wireless Commun.*, vol. 30, no. 2, pp. 122–129, Apr. 2023.

[8] G. Pan, J. Ye, J. An, and M.-S. Alouini, "Latency versus reliability in LEO mega-constellations: Terrestrial, aerial, or space relay," *IEEE Trans. Mobile Comput.*, vol. 22, no. 9, pp. 5330–5345, Sep. 2023.

[9] K. Guo et al., "Performance analysis of hybrid satellite-terrestrial cooperative networks with relay selection," *IEEE Trans. Veh. Technol.*, vol. 69, no. 8, pp. 9053–9067, Aug. 2020.

[10] "Digital video broadcasting (DVB); system specifications for satellite services to handheld devices (SH) below 3 GHz," ETSI, Sophia Antipolis, France, ETSI TS 102 585 V1.1.2, Apr. 2008.

[11] M. Lin et al., "Integrated 5G-satellite networks: A perspective on physical layer reliability and security," *IEEE Wireless Commun.*, vol. 27, no. 6, pp. 152–159, Dec. 2020.

[12] K. An et al., "Performance analysis of multi-antenna hybrid satellite-terrestrial relay networks in the presence of interference," *IEEE Trans. Commun.*, vol. 63, no. 11, pp. 4390–4404, Nov. 2015.

[13] K. An, M. Lin, W.-P. Zhu, Y. Huang, and G. Zheng, "Outage performance of cognitive satellite–terrestrial networks with interference constraint," *IEEE Trans. Veh. Technol.*, vol. 65, no. 11, pp. 9397–9404, Nov. 2016.

[14] K. Guo et al., "On the performance of the uplink satellite multiterrestrial relay networks with hardware impairments and interference," *IEEE Syst. J.*, vol. 13, no. 3, pp. 2297–2308, Sep. 2019.

[15] Z. Lin, M. Lin, J.-B. Wang, T. de Cola, and J. Wang, "Joint beamforming and power allocation for satellite-terrestrial integrated networks with non-orthogonal multiple access," *IEEE J. Sel. Topics Signal Process.*, vol. 13, no. 3, pp. 657–670, Jun. 2019.

[16] Q. Huang, M. Lin, W.-P. Zhu, S. Chatzinotas, and M.-S. Alouini, "Performance analysis of integrated satellite-terrestrial multiantenna relay networks with multiuser scheduling," *IEEE Trans. Aerosp. Electron. Syst.*, vol. 56, no. 4, pp. 2718–2731, Aug. 2020.

[17] Q. Huang, M. Lin, J.-B. Wang, T. A. Tsiftsis, and J. Wang, "Energy efficient beamforming schemes for satellite-aerial-terrestrial networks," *IEEE Trans. Commun.*, vol. 68, no. 6, pp. 3863–3875, Jun. 2020.

[18] K. Guo, C. Dong, and K. An, "NOMA-based cognitive satellite terrestrial relay network: Secrecy performance under channel estimation errors and hardware impairments," *IEEE Internet Things J.*, vol. 9, no. 18, pp. 17334–17347, Sep. 2022.

[19] H. Shuai, K. Guo, K. An, Y. Huang, and S. Zhu, "Transmit antenna selection in NOMA-based integrated satellite-HAP-terrestrial networks with imperfect CSI and SIC," *IEEE Wireless Commun. Lett.*, vol. 11, no. 8, pp. 1565–1569, Aug. 2022.

[20] K. Guo, K. An, F. Zhou, T. A. Tsiftsis, G. Zheng, and S. Chatzinotas, "On the secrecy performance of NOMA-based integrated satellite multiple-terrestrial relay networks with hardware impairments," *IEEE Trans. Veh. Technol.*, vol. 70, no. 4, pp. 3661–3676, Apr. 2021.

[21] J. Xu, L. Duan, and R. Zhang, "Surveillance and intervention of infrastructure-free mobile communications: A new wireless security paradigm," *IEEE Wireless Commun.*, vol. 24, no. 4, pp. 152–159, Aug. 2017.

[22] K. Guo et al., "Physical layer security for multiuser satellite communication systems with threshold-based scheduling scheme," *IEEE Trans. Veh. Technol.*, vol. 69, no. 5, pp. 5129–5141, May 2020.

[23] B. Li, Z. Fei, Z. Chu, F. Zhou, K.-K. Wong, and P. Xiao, "Robust chance-constrained secure transmission for cognitive satellite–terrestrial networks," *IEEE Trans. Veh. Technol.*, vol. 67, no. 5, pp. 4208–4219, May 2018.

[24] V. Bankey, V. Singh, and P. K. Upadhyay, "Physical layer secrecy of NOMA-based hybrid satellite-terrestrial relay networks," in *Proc. IEEE WCNC*, May 2020, pp. 1–6.

[25] V. Bankey and P. K. Upadhyay, "Physical layer security of multiuser multirelay hybrid satellite-terrestrial relay networks," *IEEE Trans. Veh. Technol.*, vol. 68, no. 3, pp. 2488–2501, Mar. 2019.

[26] K. Guo, M. Lin, B. Zhang, J. Ouyang, and W.-P. Zhu, "Secrecy performance of satellite wiretap channels with multi-user opportunistic scheduling," *IEEE Wireless Commun. Lett.*, vol. 7, no. 6, pp. 1054–1057, Dec. 2018.

[27] H. Zhang, P. Yue, S. Wang, G. Pan, and J. An, "On secure uplink transmissions in satellite-aerial systems," *IEEE Trans. Aerosp. Electron. Syst.*, vol. 59, no. 4, pp. 4666–4673, Aug. 2023.

[28] K. Guo, X. Li, M. Alazab, R. H. Jhaveri, and K. An, "Integrated satellite multiple two-way relay networks: Secrecy performance under multiple eves and vehicles with non-ideal hardware," *IEEE Trans. Intell. Veh.*, vol. 8, no. 2, pp. 1307–1318, Feb. 2023.

[29] Z. Lin, M. Lin, B. Champagne, W.-P. Zhu, and N. Al-Dhahir, "Secure beamforming for cognitive satellite terrestrial networks with unknown eavesdroppers," *IEEE Syst. J.*, vol. 15, no. 2, pp. 2186–2189, Jun. 2021.

[30] M. Lin, Z. Lin, W.-P. Zhu, and J.-B. Wang, "Joint beamforming for secure communication in cognitive satellite terrestrial networks," *IEEE J. Sel. Areas Commun.*, vol. 36, no. 5, pp. 1017–1029, May 2018.

[31] J. Xu, L. Duan, and R. Zhang, "Proactive eavesdropping via jamming for rate maximization over Rayleigh fading channels," *IEEE Wireless Commun. Lett.*, vol. 5, no. 1, pp. 80–83, Feb. 2016.

[32] G. Hu and Y. Cai, "Legitimate eavesdropping in UAV-based relaying system," *IEEE Commun. Lett.*, vol. 24, no. 10, pp. 2275–2279, Oct. 2020.

[33] C. Zhong, X. Jiang, F. Qu, and Z. Zhang, "Multi-antenna wireless legitimate surveillance systems: Design and performance analysis," *IEEE Trans. Wireless Commun.*, vol. 16, no. 7, pp. 4585–4599, Jul. 2017.

[34] G. Hu and Y. Cai, "Proactive eavesdropping via jamming for ergodic rate maximization over wireless-powered multichannel suspicious system," *IEEE Commun. Lett.*, vol. 24, no. 8, pp. 1830–1834, Aug. 2020.

[35] G. Hu, J. Si, Y. Cai, and N. Al-Dhahir, "Intelligent reflecting surface-assisted proactive eavesdropping over suspicious broadcasting communication with statistical CSI," *IEEE Trans. Veh. Technol.*, vol. 71, no. 4, pp. 4483–4488, Apr. 2022.

[36] B. Li, Y. Yao, H. Zhang, Y. Lv, and W. Zhao, "Energy efficiency of proactive eavesdropping for multiple links wireless systems," *IEEE Access*, vol. 6, pp. 26081–26090, 2018.

[37] B. Li and K. Cui, "IRS-assisted proactive eavesdropping over fading channels based on deep reinforcement learning," *IEEE Commun. Lett.*, vol. 26, no. 8, pp. 1730–1734, Aug. 2022.

[38] R. Ma, H. Wu, J. Ou, Q. Peng, and Y. Gao, "Power and location optimzation of full-duplex relay for proactive eavesdropping networks," *IEEE Access*, vol. 8, pp. 196712–196726, 2020.

[39] J. Moon, S. H. Lee, H. Lee, and I. Lee, "Proactive eavesdropping with jamming and eavesdropping mode selection," *IEEE Trans. Wireless Commun.*, vol. 18, no. 7, pp. 3726–3738, Jul. 2019.

[40] Y. Ge and P. C. Ching, "Energy efficiency for proactive eavesdropping in cooperative cognitive radio networks," *IEEE Internet Things. J.*, vol. 9, no. 15, pp. 13443–13457, Aug. 2022.

[41] G. Hu et al., "Maxmin fairness for UAV-enabled proactive eavesdropping with jamming over distributed transmit beamforming-based suspicious communications," *IEEE Trans. Commun.*, vol. 71, no. 3, pp. 1595–1614, Mar. 2023.

[42] H. Lu, H. Zhang, H. Dai, W. Wu, and B. Wang, "Proactive eavesdropping in UAV-aided suspicious communication systems," *IEEE Trans. Veh. Technol.*, vol. 68, no. 2, pp. 1993–1997, Feb. 2019.

[43] F. Feizi, M. Mohammadi, Z. Mobini, and C. Tellambura, "Proactive eavesdropping via jamming in full-duplex multi-antenna systems: Beamforming design and antenna selection," *IEEE Trans. Commun.*, vol. 68, no. 12, pp. 7563–7577, Dec. 2020.

[44] C. Zhang, X. Miao, Y. Huang, L. Yang, and L. Tang, "Performance of multi-antenna proactive eavesdropping in 5G uplink systems," *IEEE Trans. Wireless Commun.*, vol. 22, no. 9, pp. 6078–6091, Sep. 2023.

[45] G. Hu et al., "Analysis and optimization of STAR-RIS-assisted proactive eavesdropping with statistical CSI," *IEEE Trans. Veh. Technol.*, vol. 72, no. 5, pp. 6850–6855, May 2023.

[46] K. Guo, M. Wu, X. Li, R. Liu, and J. Dai, "Proactive eavesdropping performance for integrated satellite-terrestrial relay networks," in *Proc. IEEE ICCC*, Dalian, China, Aug. 2023, pp. 1–6.

[47] R. Liu, K. Guo, K. An, and S. Zhu, "NOMA-based overlay cognitive integrated satellite-terrestrial relay networks with secondary network selection," *IEEE Trans. Veh. Technol.*, vol. 71, no. 2, pp. 2187–2192, Feb. 2022.

[48] H. Fu, Z. Sheng, A. A. Nasir, A. H. Muqaibel, and L. Hanzo, "Securing the UAV-aided non-orthogonal downlink in the face of colluding eavesdroppers," *IEEE Trans. Veh. Technol.*, vol. 71, no. 6, pp. 6837–6842, Jun. 2022.

[49] T. Bao, H. Wang, W.-J. Wang, H.-C. Yang, and M. O. Hasna, "Secrecy outage performance analysis of UAV-assisted relay communication systems with multiple aerial and ground eavesdroppers," *IEEE Trans. Aerosp. Electron. Syst.*, vol. 58, no. 3, pp. 2592–2600, Jun. 2022.

[50] Z. Liu, S. Wang, Y. Liu, Y. Wang, X. Guan, and D. Niyato, "Robust secure transmission and power transfer in heterogeneous networks with confidential information," *IEEE Trans. Veh. Technol.*, vol. 69, no. 10, pp. 11192–11205, Oct. 2020.
[51] K. Guo and K. An, "On the performance of RIS-assisted integrated satellite-UAV-terrestrial networks with hardware impairments and interference," *IEEE Wireless Commun. Lett.*, vol. 11, no. 1, pp. 131–135, Jan. 2022.
[52] P. K. Sharma, P. K. Upadhyay, D. B. Costa, P. S. Bithas, and A. G. Kanatas, "Performance analysis of overlay spectrum sharing in hybrid satellite-terrestrial systems with secondary network selection," *IEEE Trans. Wireless Commun.*, vol. 16, no. 10, pp. 6586–6601, Oct. 2017.
[53] J. Arnau, D. Christopoulos, S. Chatzinotas, C. Mosquera, and B. Ottersten, "Performance of the multibeam satellite return link with correlated rain attenuation," *IEEE Trans. Wireless Commun.*, vol. 13, no. 11, pp. 6286–6299, Nov. 2014.
[54] A. Abdi, W. C. Lau, M.-S. Alouini, and M. Kaveh, "A new simple model for land mobile satellite channels: First- and second-order statistics," *IEEE Trans. Wireless Commun.*, vol. 2, no. 3, pp. 519–528, May 2003.
[55] I. S. Gradshteyn and I. M. Ryzhik, *Table of Intergals, Series, and Products.*, 7th ed. Amsterdam, The Netherlands: Academic Press, 2007.
[56] X. Li, H. Liu, G. Li, Y. Liu, M. Zeng, and Z. Ding, "Effective capacity analysis of AmBC-NOMA communication systems," *IEEE Trans. Veh. Technol.*, vol. 701, no. 10, pp. 11257–11261, Oct. 2022.
[57] X. Li, M. Zhao, Y. Liu, L. Li, Z. Ding, and A. Nallanathan, "Secrecy analysis of ambient backscatter NOMA systems under I/Q imbalance," *IEEE Trans. Veh. Technol.*, vol. 69, no. 10, pp. 12286–12290, Oct. 2020.
[58] Y. Zhang, X. Jiang, C. Zhong, and Z. Zhang, "Performance of proactive eavesdropping in dual-hop relaying systems," in *Proc. IEEE Globecom Workshops*, Singapore, Jan. 2018, pp. 1–6.

ZHEPING WU received the B.S. degree from Space Engineering University, Beijing, China, in 2022. He is currently pursuing the Ph.D. degree with Naval Submarine Academy. His research interests include on satellite–terrestrial networks, proactive eavesdropping networks, covert underwater acoustic communication, and underwater acoustic communication network.

KEFENG GUO received the B.S. degree from the Beijing Institute of Technology, Beijing, China, in 2012, and the Ph.D. degree from Army Engineering University, Nanjing, China, in 2018.

He is a Lecturer with the School of Space Information, Space Engineering University. He is also an Associate Professor with the College of Electronic and Information Engineering, Nanjing University of Aeronautics and Astronautics. He has authored or coauthored more than 90 research papers in international journals and conferences. His research interests focus on cooperative relay networks, MIMO communications systems, multiuser communication systems, satellite communication, hardware impairments, cognitive radio, NOMA technology, and physical-layer security. He was a recipient of Exemplary Reviewer of IEEE TRANSACTIONS ON COMMUNICATIONS in 2022. He was the recipient of the Outstanding Ph.D. Thesis Award of Chinese Institute of Command and Control in 2020. He also was the recipient of the Excellent Ph.D. Thesis Award of Jiangsu Province, China, in 2020. He also serves as an Editor on the editorial board for the *EURASIP Journal on Wireless Communications and Networking*. He was the Guest Editor of the special issue on Integration of Satellite–Aerial–Terrestrial Networks of *Sensors* and the special issue on Recent Advances and Challenges of Satellite and Aerial Communication Networks of *Electronics*. He has been the TPC member of many IEEE sponsored conferences, such as IEEE ICC, IEEE GLOBECOM, and IEEE WCNC.

XINGWANG LI (Senior Member IEEE) received the M.Sc. degree from the University of Electronic Science and Technology of China in 2010, and the Ph.D. degree from the Beijing University of Posts and Telecommunications in 2015. From 2010 to 2012, he was working with Comba Telecom Ltd., Guangzhou, China, as an Engineer. He spent one year from 2017 to 2018 as a Visiting Scholar with Queens University Belfast, Belfast, U.K. He is currently an Associate Professor with the School of Physics and Electronic Information Engineering, Henan Polytechnic University, Jiaozuo, China. His research interests include span wireless communication, intelligent transport system, artificial intelligence, and Internet of Things. He was a recipient of Exemplary Reviewer of IEEE TRANSACTIONS ON COMMUNICATIONS and *Journal of Electronics & Information Technology*. He is on the editorial board of IEEE TRANSACTIONS ON INTELLIGENT TRANSPORTATION SYSTEMS, IEEE TRANSACTIONS ON VEHICULAR TECHNOLOGY, IEEE SYSTEMS JOURNAL, and IEEE SENSORS JOURNAL. He has serviced as the Guest Editor for the special issue on Integrated Sensing and Communications for 6G IoE of IEEE INTERNET OF THINGS JOURNAL, Computational Intelligence and Advanced Learning for Next-Generation Industrial IoT of IEEE TRANSACTIONS ON NETWORK SCIENCE AND ENGINEERING, and "AI driven Internet of Medical Things for Smart Healthcare Applications: Challenges, and Future Trends" of the IEEE JOURNAL OF BIOMEDICAL AND HEALTH INFORMATICS. He has served as many TPC members, such as IEEE ICC and GLOBECOM.

YU-DONG ZHANG (Senior Member, IEEE) received the Ph.D. degree from Southeast University, Nanjing, China, in 2010. From 2010 to 2012, he was a Postdoctoral Researcher with Columbia University, New York, NY, USA, and an Assistant Research Scientist with RFMH, New York, from 2012 to 2013. From 2013 to 2017, he was a Full Professor with Nanjing Normal University, Nanjing. He is currently a Professor with the University of Leicester, Leicester, U.K. His research interests include deep learning and medical image analysis.

MINGFU ZHU (Member, IEEE) received the B.Sc. degree from Tianjin University, Tianjin, China, in 2000, the M.Sc. degree from East China Normal University, Shanghai, China, in 2004, and the Ph.D. degree from the University of California at Los Angeles, Los Angeles, CA, USA, in 2007. From 2011 to 2013, he was working as an Executive Director with Mayyard Photoelectric Technology Company Ltd., Ningbo, China. In 2013, he has founded and served as the Chairman of Hebei National Optoelectronics Technology Company Ltd., Hebei, China. He is currently the Chairman of Henan Chuangzhi Technology Company Ltd., and the General Manager of Henan Chuitian Technology Company Ltd., Hebei. He is currently a Full Professor with the School of Computer Science and Technology, Henan Polytechnic University. His research interests include chip packaging and intelligent light development and manufacturing. With innovative ideas, intelligent lights are used to build IOL, integrate IOL into IoT, and upgrade to 5G IoT. By building scientific research platforms and manufacturing bases, 5G industry ecosystem is built to interact with upstream and downstream enterprises. He was the recipient of several awards and achievements, which include the excellent builder for the socialist cause with Chinese characteristics, Special Government Allowance Under the State Council, and leading talents in Science and Technology Innovation of National Ten Thousand Talents Plan. He was a member of Henan CPPCC and the Vice President of the Henan Euro-American Alumni Association. He is also the President of the Henan Alumni Association of Tianjin University and the Director of Henan Mechanical Engineering Society.

HOUBING SONG (Fellow, IEEE) received the Ph.D. degree in electrical engineering from the University of Virginia, Charlottesville, VA, USA, in August 2012.

He is currently a tenured Associate Professor, the Director of the NSF Center for Aviation Big Data Analytics (Planning), an Associate Director for Leadership of the DOT Transportation Cybersecurity Center for Advanced Research and Education (Tier 1 Center), and the Director of the Security and Optimization for Networked Globe Laboratory (SONG Lab), University of Maryland at Baltimore County (UMBC), Baltimore, MD, USA. Prior to joining UMBC, he was a tenured Associate Professor of Electrical Engineering and Computer Science with Embry-Riddle Aeronautical University, Daytona Beach, FL, USA. He is the editor of eight books, the author of more than 100 articles and the inventor of two patents. His research interests include cyber–physical systems/Internet of Things, cybersecurity and privacy, and AI/machine learning/big data analytics. His research has been sponsored by federal agencies (including National Science Foundation, National Aeronautics and Space Administration, U.S. Department of Transportation, and Federal Aviation Administration, among others) and industry. His research has been featured by popular news media outlets, including IEEE GlobalSpec's Engineering360, Association for Uncrewed Vehicle Systems International, Security Magazine, CXOTech Magazine, Fox News, U.S. News & World Report, The Washington Times, and New Atlas. He was a recipient of 10+ Best Paper Awards from major international conferences, including IEEE CPSCom-2019, IEEE ICII 2019, IEEE/AIAA ICNS 2019, IEEE CBDCom 2020, WASA 2020, AIAA/IEEE DASC 2021, IEEE GLOBECOM 2021, and IEEE INFOCOM 2022. He has been a Highly Cited Researcher identified by Clarivate in 2021 and 2022 and a Top 1000 Computer Scientist identified by Research.com. He received Research.com Rising Star of Science Award in 2022 (World Ranking: 82; U.S. Ranking: 16). He has been serving as an Associate Editor for IEEE TRANSACTIONS ON ARTIFICIAL INTELLIGENCE since 2023, IEEE INTERNET OF THINGS JOURNAL since 2020, IEEE TRANSACTIONS ON INTELLIGENT TRANSPORTATION SYSTEMS since 2021, and IEEE JOURNAL ON MINIATURIZATION FOR AIR AND SPACE SYSTEMS since 2020. He was an Associate Technical Editor for *IEEE Communications Magazine* from 2017 to 2020. He is an IEEE Fellow (for contributions to big data analytics and integration of AI with Internet of Things), and an ACM Distinguished Member (for outstanding scientific contributions to computing). He has been an ACM Distinguished Speaker since 2020 and an IEEE Vehicular Technology Society Distinguished Lecturer since 2023.

MIN WU received the M.S. degree from Space Engineering University, Beijing, China, in 2021, where she is currently pursuing the Ph.D. degree. Her research interests include on satellite–terrestrial networks, RIS-assisted wireless communication systems, multiuser communication systems, and deep reinforcement learning.